

JGR Atmospheres

RESEARCH ARTICLE

10.1029/2023JD039868

Key Points:

- The Ural ridge regime and weak polar vortex are more frequent and persistent following low autumn sea ice in the Nordic seas
- The long-duration Ural and Greenland ridge regimes are followed by cold snaps in East Asia and the eastern US
- Cold anomalies occur more frequently in Canada with increasing occurrences of the long-duration Ural trough regimes

Correspondence to:

S. Fan,

Songmiao.Fan@noaa.gov

Citation:

Fan, S., Chen, X., & Cohen, J. (2024). Boreal winter extratropical weather regime changes during 1979–2019 and their weather impacts and possible linkages to sea-ice in the Nordic seas. *Journal of Geophysical Research: Atmospheres, 129*, e2023JD039868. https://doi.org/10.1029/2023JD039868

Received 22 AUG 2023 Accepted 10 APR 2024

Author Contributions:

Conceptualization: Songmiao Fan
Data curation: Songmiao Fan
Formal analysis: Songmiao Fan
Investigation: Songmiao Fan
Methodology: Songmiao Fan
Resources: Songmiao Fan
Software: Songmiao Fan
Validation: Songmiao Fan
Visualization: Songmiao Fan
Writing – original draft: Songmiao Fan
Writing – review & editing:
Songmiao Fan, Xiaodan Chen,
Judah Cohen

© 2024 The Author(s). This article has been contributed to by U.S. Government employees and their work is in the public domain in the USA.

This is an open access article under the terms of the Creative Commons

terms of the Creative Commons
Attribution License, which permits use,
distribution and reproduction in any
medium, provided the original work is
properly cited.

Boreal Winter Extratropical Weather Regime Changes During 1979–2019 and Their Weather Impacts and Possible Linkages to Sea-Ice in the Nordic Seas

Songmiao Fan¹, Xiaodan Chen², and Judah Cohen^{3,4}

¹NOAA Geophysical Fluid Dynamics Laboratory, Princeton, NJ, USA, ²Department of Atmospheric and Oceanic Sciences, Institute of Atmospheric Sciences, Fudan University, Shanghai, China, ³Atmospheric and Environmental Research Inc, Lexington, MA, USA, ⁴Massachusetts Institute of Technology, Cambridge, MA, USA

Abstract Previous studies have suggested possible connections between the decreasing Arctic sea-ice and long-duration (>5 days, LD) cold weather events in Eurasia and North America. Here we document the occurrences of weather regimes in winter by their durations, based on the empirical orthogonal function analyses of the daily geopotential height fields at 500 hPa (z500) for the months of November–March 1979–2019. Significant changes in the occurrence frequency and persistence of Ural ridge (UR) and weak stratospheric polar vortex (PV) were found between winters following high and low autumn sea-ice covers (SIC) in the Barents and Kara seas. It is shown that a strengthening of the UR is accompanied with a weakening of the PV, and a weak PV favors Greenland ridge (GR). Cold spells in East Asia persist for 5 more days after an LDUR. Cold spells from Canada to the U.S. occur 2–5 days after an LD Ural trough (UT) and are associated with a z500 anomaly dipole centered over Alaska (+) and Hudson Bay (–). Cold spells in the eastern U.S. occur 1–4 days after an LDGR due to circulations resembling the Pacific-North America pattern. Increased occurrences of UR in winter are associated with a decreased eastward propagation of synoptic waves from the North Atlantic to Japan and the North Pacific.

Plain Language Summary Analyses of observations show more frequent occurrences of long-duration events of Ural ridge (UR), Greenland ridge (GR) and weak polar vortex (PV) in winter tend to follow low autumn sea ice cover (SIC) in the Barents and Kara Seas, and less frequent for Ural trough (UT) and strong PV. Long-duration UR (GR or UT) events are followed by cold snaps in East Asia (the eastern US or Canada). Long-term natural or anthropogenic warming in the Arctic and decreasing autumn SIC may cause more frequent cold air outbreaks in East Asia and the eastern US in winter, but less in Canada.

1. Introduction

It was hypothesized that the reduction of Arctic sea-ice covers (SIC) is linked to extreme events in the mid latitudes (Francis & Vavrus, 2012). By this hypothesis, amplified Arctic warming causes a decrease of the meridional temperature gradient and thus a slow-down of the zonal wind in the mid latitudes, which then leads to more waviness of the jet stream and more cold air excursions to the south. For example, warm Arctic episodes were found to be linked with increased frequency of extreme winter weather in the United States (Cohen et al., 2018) and in Eurasia (e.g., Mori et al., 2014; Zhang et al., 2012). In more recent studies (Chen et al., 2018; Francis et al., 2018, 2020; Luo et al., 2018; Yao et al., 2017), the extremes were attributed to the occurrences of long duration events (LDEs). For instance, observational analyses reveal that the warming in the Barents–Kara Seas (BKS) related to the recent decline of winter SIC has been accompanied by a large increase in the mean duration of the Ural blocking and associated cold extreme events (Chen et al., 2018; Luo et al., 2018; Yao et al., 2017). Ural blocking causes warm air intrusion into the Arctic, which in turn may lead to further decreases in SIC in the Barents Sea, because increased downward longwave radiation and sensible heat flux melts sea ice and southerly winds push sea ice poleward (Chen et al., 2018; Fan & Yang, 2017; Gong & Luo, 2017; Lee et al., 2017; Luo et al., 2016, 2017; Tyrlis et al., 2019; You et al., 2022).

Large-scale circulation anomalies in the troposphere may propagate to, and originate from, the stratosphere (e.g., Nishi et al., 2010; Perlwitz & Graf, 2001; Woo et al., 2015). A stratospheric pathway linking mid-latitude climate to the BKS sea-ice loss has been proposed previously and explored based on observations and modeling studies in numerous publications (e.g., X. Chen, et al., 2021; Garcia-Serrano et al., 2015; Kim et al., 2014; Kim &

FAN ET AL. 1 of 21

Kim, 2020; McKenna et al., 2018; Nakamura et al., 2015, 2016; Peings et al., 2023; Sun et al., 2015; Zhang et al., 2018). A weak polar vortex is more likely to occur in response to the reduction of autumn SIC in the BKS, which may persist into winter months. A negative phase shift of the winter Arctic oscillation (AO) and North Atlantic oscillation (NAO) may have occurred due to the SIC reduction in late autumn (Nakamura et al., 2015), which weakens the meridional potential vorticity gradient and leads to more persistent blocking over Eurasia, Greenland, and northwestern North America (Luo et al., 2019).

Despite many studies cited above, the Arctic linkage to extreme weather remains uncertain (Barnes, 2013; Barnes & Screen, 2015; Cohen et al., 2020; Francis, 2017; McCusker et al., 2016). For instance, Blackport et al. (2019) found robust support for anomalous atmospheric circulation simultaneously driving cold midlatitude winters and mild Arctic conditions, and reduced sea ice having a minimal influence on severe midlatitude winters (based on monthly mean temperatures). Perhaps the causal effects of sea ice variability on midlatitude winter climate are much weaker than suggested by statistical associations, evident in observations and coupled models, because the statistics are inflated by the effects of atmospheric circulation variability on sea ice (Blackport & Screen, 2021).

Furthermore, the Arctic trends and associated temperature trends in the midlatitude observed from 1988/89 to 2011/12 have reversed from 2012 to 2019, suggesting that observed periods of strong correlation are an artifact of internal variability (Blackport & Screen, 2020) or that causal relationships are intermittent, being strong at times and weak at other times (Overland et al., 2021). However, these conclusions were based on time-averaged observations and do not necessarily contradict the increase of LDEs as claimed. The LDEs are relatively rare and have limited effects on monthly mean temperatures, even less on seasonal averages. Cold extremes can occur in some years without reversing the long-term winter warming in the midlatitudes although their magnitude may be damped by higher temperatures in the Arctic.

The reversal of trends from 2012 to 2019 was attributed to decadal variations of the sea surface temperature (SST), that is, the SST tripole pattern in the North Atlantic Ocean (Y. Chen, Luo, Zhong, & Yao, 2021). A positive phase of the tripole (meridional SST -+- anomaly pattern) favors occurrence of the positive phase of the North Atlantic Oscillation (NAO+) (Peng et al., 2002), while a negative phase of the tripole (+-+) may cause a negative phase of the NAO (NAO-) (Peng et al., 2003). The variations of the winter mean NAO index and the SST tripole index are strongly positively correlated (Y. Chen, Luo, Zhong, & Yao, 2021). The NAO is known to modulate surface temperatures in northern Eurasia and SIC in the Barents Sea (references cited in Y. Chen, Luo, Zhong, & Yao, 2021). In winters with more frequent negative than positive AO/NAO events, when the background meridional potential vorticity gradient is small the East Asian cold extremes can even occur in the absence of large negative SIC anomalies (Luo et al., 2019).

Interdecadal Pacific Oscillation (IPO) and Atlantic multidecadal oscillation (AMO) may also modulate the extratropical weather regimes, and cause substantial decadal variability in the occurrence of warm Arctic-cold Eurasia events (Luo et al., 2022). In particular, cold anomalies occur in Central Eurasia during the negative phase of IPO (IPO-) and warm anomalies over the BKS during the positive phase of AMO (AMO+) (Luo et al., 2022). Tropical SST anomalies and associated convective heating may influence Arctic temperature and sea ice by modulation of poleward energy transport (Lee et al., 2011). Polar and extratropical circulations may respond to the quasi-biennial oscillation and El Niño-Southern Oscillation (Kumar et al., 2022; Labe et al., 2019).

According to previous studies the most significant weather regimes that affect temperature and precipitation in North America include both the positive and negative phases of the NAO, Pacific-North America (PNA), and Western Pacific (WP) patterns (e.g., Leathers et al., 1991; Robertson & Ghil, 1999; Thompson & Wallace, 2001; Wise et al., 2015; Yang et al., 2022). It is well known that these circulation patterns are influenced by tropical oscillations, such as the Madden-Julian Oscillation and El Nino Southern Oscillation (e.g., Jenney et al., 2019; Riddle et al., 2013; Roundy et al., 2010; Xiang et al., 2021). In this study it is suggested that the weather regimes centered over the Urals and Greenland may also influence North America, but not directly as the former regimes.

Interannual variations of weather regimes may result from the internal variability of dynamics (Overland et al., 2021), various tropical oscillations (Cassou, 2008; Lin et al., 2015; Luo et al., 2022; Matsumura & Kosaka, 2019; Mori & Watanabe, 2008; Riddle et al., 2013; Roundy et al., 2010; Sung et al., 2019; Warner

FAN ET AL. 2 of 21

et al., 2020; Zhou et al., 2012), and stratospheric sudden warmings (Butler et al., 2017). Major volcanic eruptions (El Chichon in 1982 and Pinatubo in 1991) may also alter the global climate/weather patterns (Groisman, 1992; Robock, 2000; Stenchikov et al., 2002). High latitude snow cover in late autumn and early winter may also influence the extratropical weather regimes in winter (e.g., Cohen, Screen, et al., 2014; Furtado et al., 2016; Vavrus et al., 2017).

A clear path forward is then to explore possible processes linking the Arctic and midlatitudes, such as the modulation of weather regimes by the reduction of Arctic sea-ice (Overland et al., 2016). These processes work together with above-mentioned tropical and stratospheric processes amid internal variations over a range of timescales. A Bayesian approach is thus recommended that considers conditional dependency of weather extremes on Arctic SIC (Overland, 2016), if observations are sufficiently long. Model simulations using prescribed initial and boundary conditions have been proven useful for process studies but may be biased due to inaccurate representation of physical processes and numerical noises, which may lead to instability and large internal variability. Composite averaging of observations at different timescales is a useful technique provided that sample sizes are large for a detectable signal-to-noise ratio. A short observational record combined with a nonstationary relationship has caused many to be skeptical of any report of linkages between Arctic sea-ice and mid-latitude weather trends. Extending observational data using reanalysis before the satellite era (1979-present) may not be enough to decrease the doubt because large ensemble model simulations have shown large internal variabilities, such that the effects of SIC changes on the PV cannot be confirmed with hundreds of ensemble members (Peings et al., 2021; Sun et al., 2022). Furthermore, it has been shown in model simulations that stratospheric PV responses to SIC reductions in the BKS and the Chukchi-Bering Seas are opposite in sign and the combined effect is relatively small (McKenna et al., 2018; Sun et al., 2015).

With the above caveat we present here analyses that show trends of boreal winter weather regimes during 1979–2019 and their strong associations with autumn SIC from the Greenland and Norwegian Seas to the Barents and Kara Seas (i.e., mainly the Nordic seas). Our analyses support previous studies that the decreasing Arctic SIC changes the frequency of LDEs with large impact on air temperature in Eurasia and North America. The data and analysis methods are presented in Section 2. The extratropical weather regimes in winter are described in Section 3, including their changes conditional on SIC in the Nordic seas during 1979–2019. The lagged impacts of these changes on mid-latitude circulations and temperatures are discussed in Sections 4 and 5 respectively. Results and conclusions are summarized in Section 6.

2. Data and Methods

In this study the weather regimes were classified based on sectional empirical orthogonal function (EOF) analysis of daily z500 fields. Daily z500 anomalies were calculated by removing the long-term (1979–2019) average for each day of the year. The EOFs of z500 anomalies were calculated separately for the PNA domain (PNA sector: $150^{\circ}\text{E}-60^{\circ}\text{W}$, $30^{\circ}\text{N}-90^{\circ}\text{N}$) and the Atlantic-Eurasia domain (AEA sector: $60^{\circ}\text{W}-150^{\circ}\text{E}$, $30^{\circ}\text{N}-90^{\circ}\text{N}$). The time series of each principal component (PC) corresponding to each EOF was normalized by the standard deviation over all data points (November 1 to March 31 and 1979 to 2019). The geopotential height, air temperature, and wind data were obtained from the National Center for Environmental Prediction and Department of Energy (NCEP/DOE) reanalysis (Kanamitsu et al., 2002). The monthly sea-ice data were provided by the National Snow and Ice Data Center at the University of Colorado Boulder (Meier et al., 2013; Peng et al., 2013). In additional analyses we used NCEP and National Center for Atmospheric Research (NCAR) reanalysis data for z500 (Kalney et al., 1996), and the Hadley Center SIC data set for the extended period of 1948–2019 (Rayner et al., 2003). For the purpose of intercomparison, conventional daily teleconnection index data for NAO, PNA, and WP were obtained from the NOAA Earth System Research Laboratory.

In order to diagnose processes responsible for possible Arctic-middle latitude tele-connection, composite maps of z500 and air temperature at 925 hPa (T925) were constructed for each weather regime at a range of lead and lag times. Similarly composite maps of height anomaly fields at 100 hPa (z100) were also constructed to show the circulation patterns in the lower stratosphere. A polar vortex index (PVI) was calculated as the daily anomaly of z100 averaged over the polar cap (70°N–90°N) normalized by the standard deviation of the daily z100 anomalies over the entire data period and the sign is reversed (i.e., positive PVI for negative z100 anomaly), following Barnes et al. (2019).

FAN ET AL. 3 of 21

onlinelibrary.wiley.com/doi/10.1029/2023JD039868 by Universitaet Leipzig, Wiley Online Library on [04/07/2024]. See

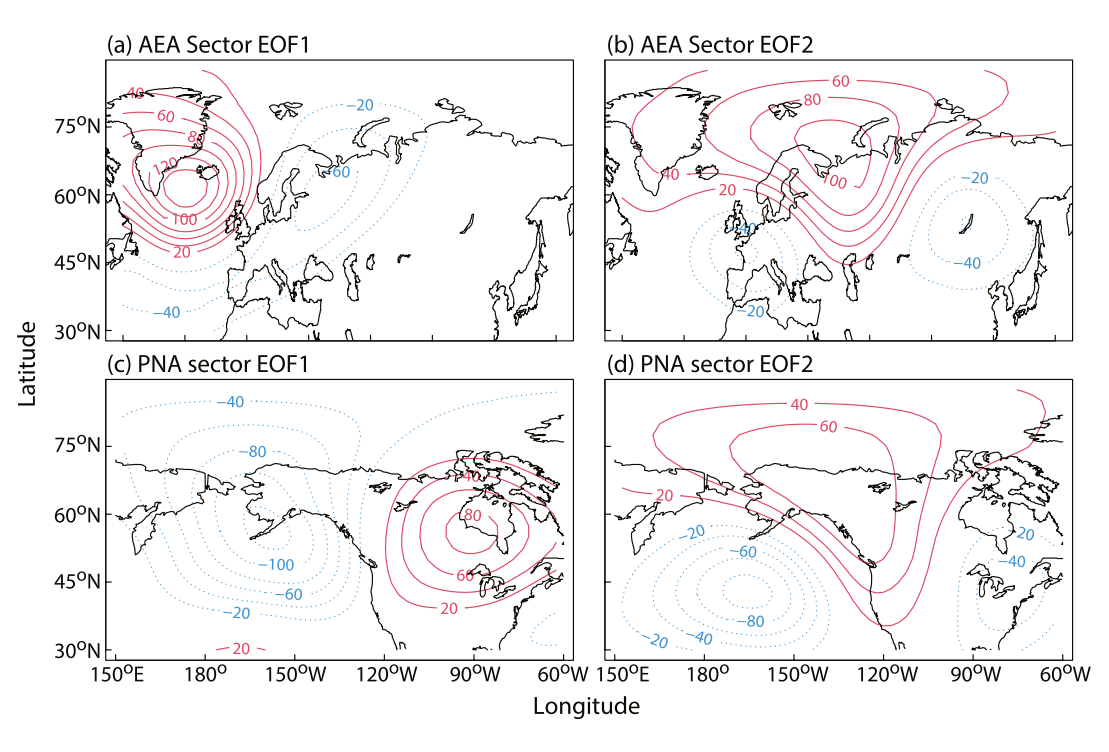


Figure 1. The first two EOFs for the Atlantic-Eurasia sector and for Pacific-North America sector, respectively. Contour lines show z500 anomalies in gpm.

3. Extratropical Weather Regimes and Sea-Ice Changes

3.1. Characterization of Weather Regimes

It is shown in Figure 1 the first two EOFs for the AEA and PNA sectors. The first and second EOFs in the AEA sector are here called Greenland ridge (GR, Figure 1a) and Ural ridge (UR, Figure 1b), and the negative phases Greenland trough (GT) and Ural trough (UT), respectively. The first and second EOFs in the PNA sector resemble the WP and PNA patterns described in previous studies (e.g., Barnston & Livezey, 1987; Wallace & Gutzler, 1981). They are here named WP+ (Figure 1c) and PNA+ (Figure 1d), the negative phases WP- and PNA-, respectively. The GR is characterized by positive anomalies centered at 60°N and 30°W, surrounded by negative anomalies to the south and to the east (Figure 1a). The UR pattern has positive anomalies centered over the Barents Sea, extending southward to the Caspian Sea, westward to Greenland, northeastward over the Arctic Ocean, and two negative anomaly regions, one over West Europe and another over Mongolia and East Siberia (centered at Lake Baikal, Figure 1b). The WP is a dipole pattern with negative anomalies over the Bering Sea and Alaska and positive anomalies centered over the Hudson Bay (Figure 1c). The PNA consists of three anomaly centers, with positives over a region from California to Alaska and the Arctic, flanked by negatives over the midlatitude Pacific and the eastern North America, respectively (Figure 1d).

A correlation coefficient r = -0.87 was found between the time series of daily PC values for GR and the daily NAO index for the entire period (151 days × 40 years). Significant correlations were also found between the December–February (DJF) mean PC values for UR and the index for various teleconnection/weather patterns: r = -0.69, 0.92, 0.82 and 0.65 for NAO, polar-Eurasia, Eurasia-1 with a ridge over northern Scandinavia, and Eurasia-2 with a trough over the United Kingdom (UK), which respectively correspond to the first, second, sixth, and fifth modes of the rotated EOF (REOF) for DJF-mean z500 fields in the AEA sector (Barnston & Livezey, 1987; Wallace & Gutzler, 1981). The high correlations likely reflect wave propagations and eastward energy dispersion over Eurasia and the effect of time averaging when monthly or seasonal mean z500 fields are used. The correlation coefficients are r = 0.64 and 0.71 between the daily PC values and the daily WP and PNA index, respectively. There is also a significant correlation (r = 0.59) between the daily PC for WP (Figure 1c) and the daily PNA index. The pattern names WP and PNA are used here for convenience, caution is required when they are compared to studies based on the traditional definitions (Barnston & Livezey, 1987; Wallace & Gutzler, 1981).

FAN ET AL. 4 of 21

It is noted that the UR pattern (Figure 1b) resembles that of the Scandinavian pattern (SCA) based on the REOF6 of DJF-mean z500 (not shown) or the REOF6/7 of DJF-mean z300 (Pang et al., 2023; Wang & Tan, 2020). The anticyclonic center of UR (Figure 1b) is located over the Barents Sea, and the eastern cyclonic center over Lake Baikal, both of which are shifted about 20° eastward from the classical definition of SCA. However, greater resemblance is found between the composite mean z500 of the UR and z300 of the SCA patterns for their individual events. In fact, two out of five Ural blocking events are mixed with Scandinavian blocking (Murto et al., 2022). The UR patterns also show similarities with the polar-Eurasia pattern (PEU) based on the rotated EOF2 for DJF-mean z500 (Jiang et al., 2023). However, the UR pattern is based on daily z500 anomalies, which gives better representation of the large-amplitude events than the PEU pattern. There exist good overlapping of the UR and PEU events from 1979 to 2019 (not shown), where the PEU events were based on projection of the PEU pattern to daily z500 anomalies (Jiang et al., 2023).

The anticyclonic UR anomalies extend southward to the Caspian Sea, and may be associated with a blocking regime in the area adjacent to the Ural Mountains. We compared the UR events with the Ural blocking (UB) events based on a one-dimensional (1D) blocking index of Tibaldi and Molteni (1990), and diagnosed for the longitudinal sector of 30°E–90°E (Luo et al., 2018, 2019). The duration of an UB event is defined as the number of days when the daily z500 anomaly averaged over the region from 55°N–75°N and from 30°E–90°E exceeds 80 gpm within its life cycle (Luo et al., 2018). A correlation coefficient of 0.42 was found between the total number of UR and UB days in each season (NDJFM) during 1979–2019. A ridge is not always associated with a blocking regime over the Ural and Scandinavian sectors (Murto et al., 2022).

3.2. Correlations Between Ural Ridge, Polar Vortex, and Sea-Ice Changes

It is shown in Figure 2 the time series of (a) September–November (SON) mean SIC in the 30°W–90°E sector (north of 70°N), (b) DJF-mean Ural ridge index (URI = normalized PC corresponding to the UR regime), and (c) DJF-mean PVI. Significant correlations are found between the SIC and URI (-0.65), between the SIC and PVI (0.50), and between the URI and PVI (-0.64). It is worth noting that less significant correlations are found for DJF-mean SIC with URI (-0.45) and PVI (0.24). A more significant correlation (-0.71) is found between URI and PVI for November alone due to a stronger coupling between UR and PV. It is shown in previous studies that a strong or weak polar vortex in autumn may persist into winter months (Garcia-Serrano et al., 2015; Kim et al., 2014; Peings, 2019; Peings et al., 2023). These results are consistent with previous studies suggesting that the reduction of SIC in the BKS might be related to a weaker polar vortex and a strengthened ridge in the Ural Mountains and the BKS region (e.g., Kim & Kim, 2020; Zhang et al., 2018).

The time series of SIC shows a peak near 1989 and decreases linearly to the lowest value in 2012 (Figure 2, note the time is shifted by 1 year for the SON mean SIC to compare with the DJF mean URI and PVI). It is noted that the variations in URI and PVI did not follow that of SIC between 2012 and 2019 as they did in the earlier years (Figure 2), consistent with smaller effects of Arctic amplification on the mid-latitude climate in more recent years (Blackport et al., 2019) and the notion of intermittency of Arctic influence and significant contributions from simultaneous processes (Y. Chen, Luo, Zhong, & Yao, 2021; Overland et al., 2021).

3.3. Weakening of PV From UR Initiation to Maturation

Previously Ural blockings were suggested to be a driver of early-winter stratospheric warmings and weak PV over the Arctic (X. Chen et al., 2021; Peings, 2019; Peings et al., 2023). Here we examine z100 and z500 anomalies associated with the life cycles of the LDUR events (i.e., PC > 1 lasting for 6 days and longer). Figure 3 shows the composite z100 anomalies at lags -8 to 2 days from the first day of LDUR events, where lag = 0 on the first of continuous days with PC > 1. At the initiation and growth stage of a UR regime z100 anomalies increase simultaneously with z500 anomalies over the polar cap as well as the Ural region. By contrast, z100 anomalies remain nearly constant at 60-80 gpm over the polar cap from lags -8 to 2 days for a GR regime, while the ridge over Greenland grows to >200 gpm (not shown). The stippling in Figure 3 and following figures indicates grid points where the anomalies are statistically significant at the 99% confidence level based on the procedure described in Wilks (2016), which improves the field significance approach of Livezey and Chen (1983). A control criterion for the false discovery rate is set to 0.02, corresponding to a global p-value of 0.01 for rejecting the null hypothesis (Wilks, 2016).

FAN ET AL. 5 of 21

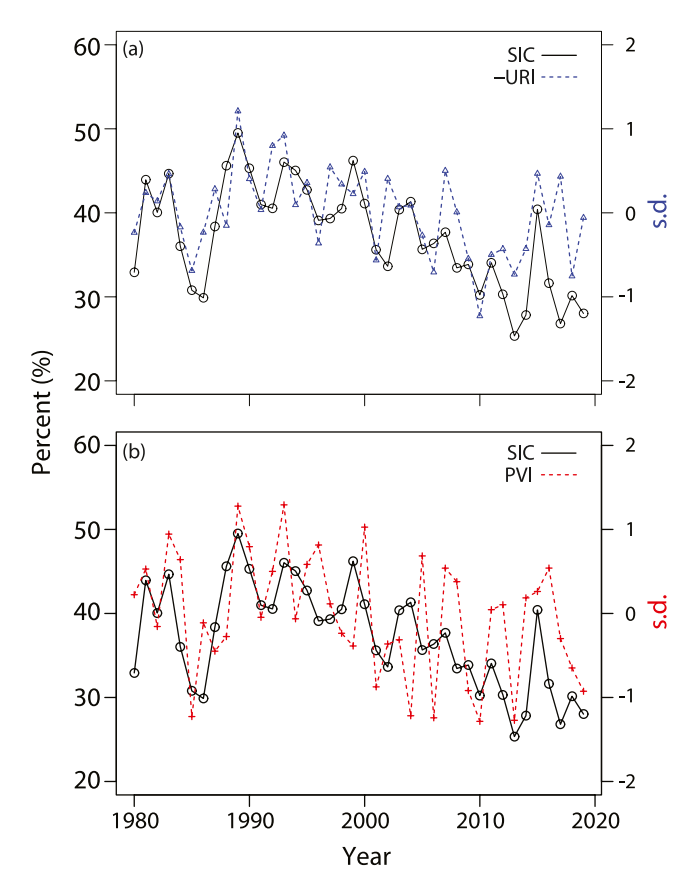


Figure 2. Time series of seasonal mean sea ice cover (SIC in SON of the preceding year, solid line) in the sector 30°W–90°E and north of 70°N compared with (a) the Ural ridge index (URI in DJF, sign inverted, blue dashed line) and (b) the polar vortex index (PVI in DJF, red dashed line). Year "1980" stands for December 1979–February 1980.

It is hypothesized that the increase of z100 over the polar cap (with peak values over 160 gpm) is contributed by the advection of Atlantic air masses into the Arctic as the UR regimes grow and mature. The relatively warm air masses move poleward between a low over southern Greenland or West Europe and a high over East Europe, which increases z100 (or thickness below 100 hPa) in the Arctic. A low centered over Lake Baikal could similarly contribute to the increase of z100 (Figure 3), to anomalies >150 gpm over the polar cap at the maturation of UR regimes (not shown). These results suggest that an LDUR event leads to a weak PV, and a weak PV may lead to a GR (see above).

Previously it was suggested that explosive cyclogenesis over the Mediterranean is a precursor of Ural blocking (Cheung et al., 2012). The warm conveyor belts associated with the cyclones with vigorous latent heating strengthen the Ural ridge by pumping up low vorticity air masses (Murto et al., 2022). The trough over West Europe (Figure 1b) and a strengthened westerly jet over the Mediterranean are indeed favorable to cyclogenesis to its north. During GR or NAO- periods, the eddy-driven jet in the upper troposphere shifts southward and merges with the subtropical jet over the Mediterranean and the storm track also shifts southward toward the Mediterranean (Athanasiadis et al., 2010; Wettstein & Wallace, 2010). A feedback loop from LDUR -> weak PV -> LDGR -> UR would cause these regimes to be simultaneously more frequent in some winters (see below). However, the link from LDGR -> UR is weak, in fact, a development of Ural blocking may occur 4–7 days after NAO+ (Luo et al., 2016). On the other hand, development of UB may be favored by a weak meridional gradient of potential vorticity during a lasting AO-/NAObackground circulation (Luo et al., 2019).

The z100 composites from lag day -8 to 2 suggest that a relatively weak PV (PVI < -0.3) also promotes short-duration (SD, 1–5 days) UR, while a relatively strong PV (PVI >0.3) promotes LDUT and SDUT, as well as LDGT and SDGT, and that the LDUR and SDGR are preceded by a neutral PV (not shown).

3.4. Weather Regime Changes by Event Duration, Conditional on Sea-Ice Changes

Long duration events have greater impact on weather, people and ecosystems (Cohen et al., 2018; Francis et al., 2018). Here we count the number of occurrences by the length of continuous days with IPCl > 1. We document winter (November–March) weather regime changes by event duration, conditional on Nordic SIC in autumn (SON, Table 1) and winter (DJF, Table A1), and on SON SIC but between two periods (1990–2004 and 2005–2019, Table A2). The event counts in 15 years are grouped into four intervals of duration (D1: 1–5, D2: 6–10, D3: 11–15, and D4: 15+ days). The counts for LDEs are shown in D2, D3 and D4, and the counts in D1 are shown for reference. The standard deviation (s.d.) is calculated from 1000 bootstrapping samples, that is, for each sample randomly selecting 15 years from the 40 years of observations. Changes that are greater than 2 s.d. are indicated by bold fonts in the tables, and are considered "statistically significant."

Table 1 shows the number of events in 15 high SON-mean SIC years and 15 low years, with 10 intermediate years neglected. From high to low SIC years, significant changes of LDEs in Table 1 include: (a) an increase of GR from 0 to 3 for D4, (b) an increase of UR from 8 to 22 for D2, (c) an increase of UR from 0 to 6 for D4, (d) a decrease of UT from 6 to 2 for D4, (e) a decrease of WP+ from 4 to 1 for D4, (f) an increase of WP- from 3 to 8 for D3, (g) a decrease of PNA+ from 19 to 13 for D2, (h) a decrease of strong PV from 6 to 2 for D4, and (i) an increase of weak PV from 3 to 7 for D2. The most striking changes are the increases of UR and weak PV events, and the decreases of UT and strong PV events, for all duration groups (D1-D4). The increases of GR are uniform for the LD groups (D2-D4). Observations show the GR frequently occurs with weak PV such as following sudden stratospheric warming events, although the mechanism is not clear (Butler et al., 2017). Increases of PNA-events found in all groups are not significant individually.

FAN ET AL. 6 of 21



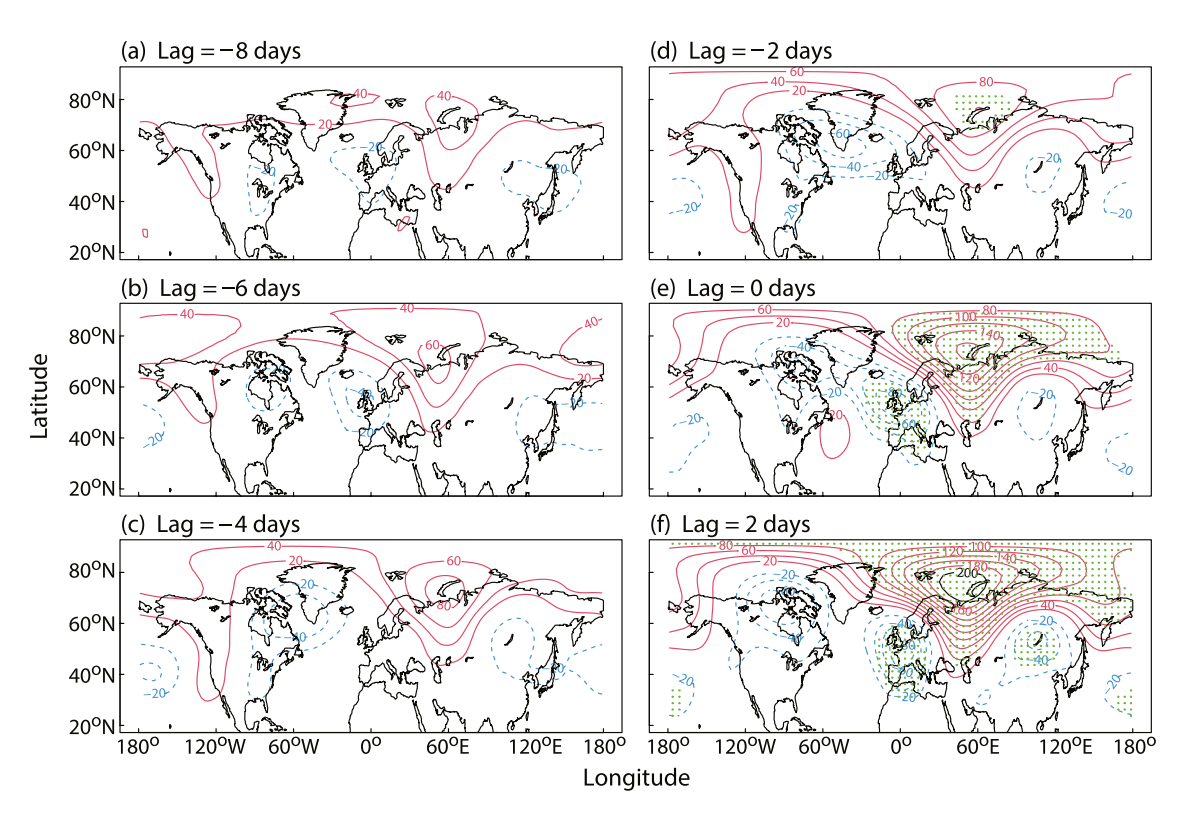


Figure 3. Composite mean of z100 anomalies (gpm) on days 8, 6, 4, 2, 0, and -2 before an LDUR event. Day 0 is the first of at least 6 days with URI >1. Stippling indicates significance at a global p-value of 1% level based on a field significance test.

Over all events (D1–D4), the UR regime occurred 5.2 (2.7) times per season with a mean duration of 6.5 (4.6) days following autumns with low (high) SIC (Table 1). In comparison, the UB regime, as diagnosed in Luo et al. (2018), occurred 5.6 (4.6) times per season with a mean duration of 5.4 (4.5) days, showing relatively smaller impacts of the autumn SIC.

Because the SIC leads the weather regimes by a few months in Table 1, the significant changes likely indicate (a) the former is a cause for the latter and/or (b) they share a common cause. The UR and weak PV changes show the same sign in all duration groups, so do the UT and strong PV changes, which strongly suggests they are mechanistically connected (see Figure 3) and both modulated by autumn SIC in the Nordic seas. On the other hand, a possible common cause remains to be established.

The UR pattern is likely a natural mode of variability, as a result of the geographical configuration of ocean, land, and ice, which may be amplified by persistent changes in SST, snow cover and sea ice. The growth of UR is forced by the warm conveyor belt originating from the warm Atlantic Ocean to the west (Murto et al., 2022), or from the Mediterranean (Cheung et al., 2012), and promoted by a cold dome over Siberia to the east (Cohen, Furtado, et al., 2014; Fletcher et al., 2009). Longwave radiation and heat fluxes from ice-free BKS amplify the UR height anomalies (X. Chen et al., 2021; Nakamura et al., 2015; Peings et al., 2023), while ice is further reduced in the BKS during a UB event (Chen et al., 2018; Gong & Luo, 2017; Luo et al., 2017). Increases of SST (~1 K) in the subarctic Atlantic Ocean, a source region of inflow water for the Barents Sea, have occurred during 1979–2019 (Fan, 2022). Episodic cooling over Siberia could have been enhanced due to a long-term increase of October snow cover (not shown) and associated increase of surface albedo. The October snow cover is correlated with the long-term trend in autumn SIC in the Nordic seas but is not with its year-to-year variations (not shown).

These trends in SST and snow cover, as well as SIC, could have together caused the composite differences in UR/ weak PV and UT/strong PV shown in Table 1. This hypothesis may be compared to a previous result of composite differences of Northern Annular Mode index between years of "low ice & high snow cover" (LI&HSC) and "high ice & low snow cover" (HI&LSC) which exceed 1 s.d. in magnitude at 100 hPa (i.e., weak PV at LI&HSC) from December to January (Furtado et al., 2016). It is interesting that the composite differences are larger than those

FAN ET AL. 7 of 21

Table 1Numbers of Events for Each Weather Regime by Durations in 15 High Ice Years (H) and 15 Low Ice Years (L), Respectively, During the Months November–March From 1979 to 2019

	D1	D2	D3	D4	D1	D2	D3	D4		
Durations (days)	1-5	6–10	11–15	15+	1–5	6–10	11–15	15+		
		GR				GT				
s.d.	5.8	3.1	1.9	1.4	9.0	4.1	2.3	0.6		
Н	48	16	4	0	79	20	6	0		
L	34	21	5	3	66	14	4	0		
	UR				UT					
s.d.	6.1	4.4	3.1	1.5	5.4	3.4	2.6	1.6		
Н	28	8	4	0	44	15	9	6		
L	41	22	9	6	35	11	5	2		
	WP+				WP-					
s.d.	7.2	3.7	2.5	1.3	6.9	3.7	2.4	1.3		
Н	51	14	5	4	27	17	3	3		
L	35	14	7	1	44	19	8	2		
		PN	A+		PNA-					
s.d.	7.8	2.6	2.1	1.6	7.7	3.6	1.9	1.8		
Н	51	19	2	1	50	11	5	4		
L	38	13	6	2	51	17	6	6		
	Strong PV				Weak PV					
s.d.	4.9	2.6	1.7	1.7	4.7	1.9	1.6	2.2		
Н	25	8	5	6	10	3	4	3		
L	14	5	2	2	15	7	6	7		

Note. Sea ice concentrations were averaged from 30°W to 90°E and north of 70°N during the preceding months September–November. Bold fonts signify a change greater than 2 standard deviations (s.d.). *High ice years:* SON'88, 98, 92, 87, 89, 93, 82, 80, 94, 03, 99, 90, 91, 97, 14. *Low ice years:* SON'12, 16, 13, 18, 85, 17, 09, 11, 84, 15, 79, 07, 01, 08, 10. *Medium ice years:* SON'00, 04, 83, 05, 06, 86, 95, 96, 81, 02.

between LI and HI or between HSC and LSC, although the mechanism for the combined effect is unknown (Furtado et al., 2016).

Similar trends for UR and UT from high to low SIC are shown in Table 1, Table A1, and Table A2, but the trends are most consistently significant in Table 1 (i.e., when SIC leads). Table A1 shows the number of events in 15 high DJF SIC years and 15 low years. From high to low SIC years, significant changes of LDEs in Table A1 include: (a) an increase of UR from 10 to 26 for D2, (b) a decrease of WP+ from 21 to 11 for D2, (c) a decrease of WP- from 19 to 11 for D2, (d) a decrease of PNA+ from 18 to 10 for D2, (e) an increase of PNA+ from 1 to 7 for D3, (f) an increase of PNA- from 10 to 19 for D2, and (g) an increase of PNA- from 2 to 6 for D3.

The decrease of PNA+ and increase of PNA— from high to low DJF-mean SIC (Table A1) is most likely related to the trends in UT and UR. Because a large fraction of the PNA+ (PNA—) is synchronized with the UT (UR) events in winter, which appears as the third mode of daily z500 in the Northern Hemisphere from November to March (EOF3-NH), in the form of a Rossby wave (wavenumber 3, not shown). By this mechanism the shifting of PNA phase may be partly attributed to the changing sea ice (Table 1 and Table A1). This is consistent with the observations and model results that a reduced Aleutian Low is more likely in winters of low SIC in the BKS (Warner et al., 2020). But it is in contrast with the hypothesis that the covariability between sea ice and the Aleutian Low originates from tropical SST and rainfall variations and their teleconnections to the extratropic (Warner et al., 2020).

Table A2 shows the number of events for two 15-year periods (1990–2004 and 2005–2019 for January year) with relatively high and low SIC (Figure 2), respectively. From the first to the second period, significant changes of LDEs in Table A2 include: (a) an increase of UR events from 8 to 23 for D2, (b) a decrease of UT events from 9 to 2 for D3, (c) a decrease of WP+ events from 17 to 8 for D2, (d) a decrease of PNA+ events from 21 to 11 for D2, (e) an increase of PNA+ events from 1 to 7 for D3, and (f) an increase of weak PV events from 2 to 6 for D2.

It is noted that the associations of UR/weak PV/GR frequencies and persistence with the SON and DJF sea ice (Table 1 and Table A1) both suggest that SIC in the Nordic seas can modify the extratropical circulations. More

coherent associations with the SON SIC do not exclude the effect of ice-free ocean in DJF. In fact, DJF- and SON-mean SIC time series are significantly correlated (r = 0.69). It is possible that the interannual variations of SON-mean SIC may better reflect the variations of surface forcing in winter because of uncertainties in ice thickness and leads, whose effects are not represented by the observed SIC variations. The surface forcing in winter work in tandem with the effect of autumn SIC (i.e., through the stratospheric pathway).

4. Lag Composites of Z500 Anomalies for Weather Regimes

Before discussing the effects of LDEs on temperature in Eurasia and North America, we show their effects on circulations that are responsible for winds associated with cold anomalies in winter. Here we focus on circulations after LDEs that have been less documented in literature. Figure 4 show composite z500 anomalies from 0 to 5 days after an LDGR (day 0 corresponds to the last day PC > 1). On day 0, a broad area of positive anomaly is located from North Canada to the subarctic Atlantic Ocean, and two connected areas of negative anomalies are centered over Scandinavia and the North Atlantic, (~40°N), respectively. A North Canada-Scandinavia dipole of z100 persists from day 0 to day 3 (not shown). A wave-train of z500 anomalies resembling the PNA+ pattern persists from day 0 to day 5, as do a ridge over Central Asia and a trough over Novaya Zemlya Island. Temperature anomalies in North America after LDGR events are thus expected to show a similar pattern to that during a PNA+ event (see below).

FAN ET AL. 8 of 21

21698996, 2024, 11, Downloaded from https://agupubs.onlinelibrary.wiley.com/doi/10.1029/2023JD039868 by Universitaet Leipzig, Wiley Online Library on [04/07/2024]. See the Terms

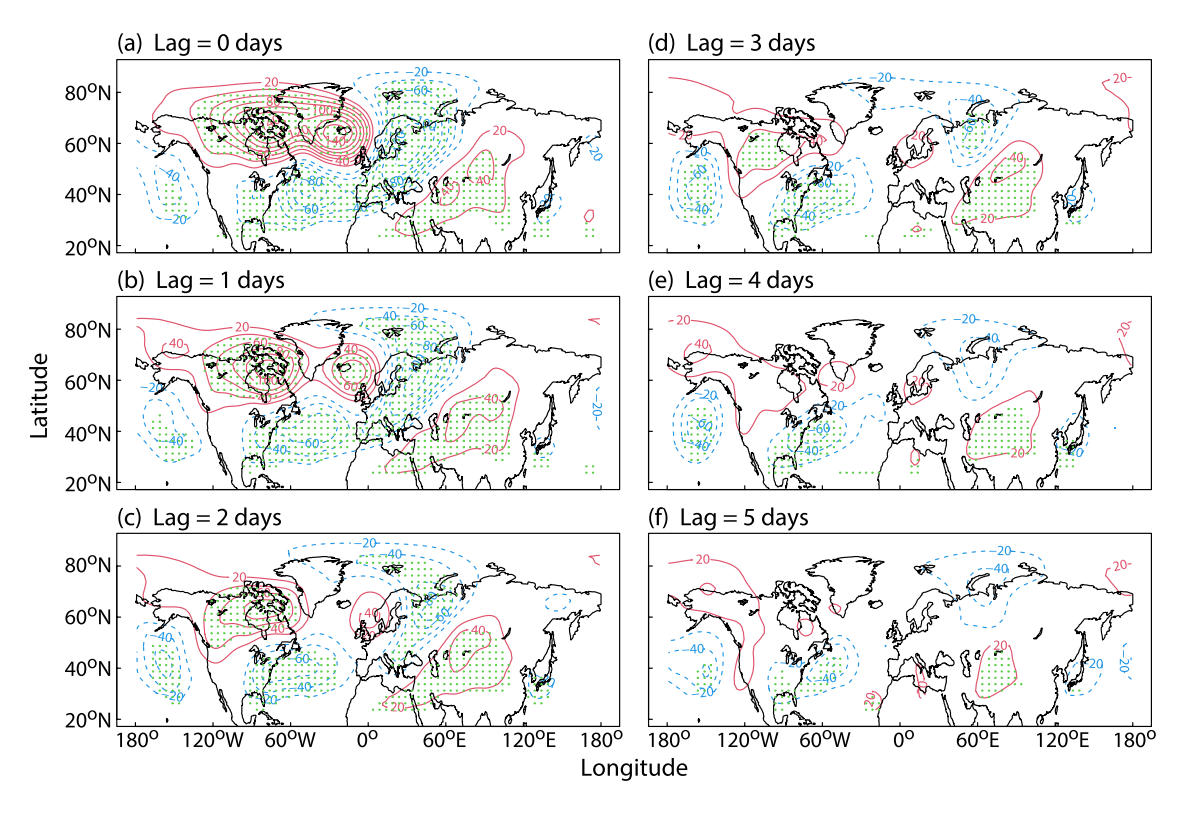


Figure 4. Composite mean of z500 anomalies (gpm) from 0 to 5 days after an LDGR event. Lag = 0 on the last of at least 6 days GR index >1. Stippling indicates significance at a global p-value of 1% level based on a field significance test.

Composite z500 anomalies from 0 to 5 days after an LDUR (Figure 5) shows a trough initially located over Siberia and shifting to East Asia as it weakens. The positive anomalies over the polar cap are much larger (\sim 150 gpm) and more persistent at 100 hPa (not shown), suggesting that a weak PV develops with an LDUR and persists at least 5 days after the event. Composites of z100 and z500 anomalies from 0 to 5 days after an LDUT (day 0 corresponds to the last day PC < -1) show opposite signed patterns of an LDUR over Eurasia, and an Alaska-Hudson Bay dipole which is a part of a wave-train from Central Pacific to North Atlantic (Figure 6). The dipole resembles a weak WP- pattern (compare panels in Figures 1c and 6), suggesting negative WP-like effects on North America temperature (see below).

5. Long-Duration Weather Regimes and Their Impact on Air Temperature

5.1. Temperature Anomalies Associated With the PNA and WP Patterns

Composite z500 anomalies during and after the LDEs indicate the winds for the advection of climatological temperature. In order to explore the effect of the weather regimes composites of air temperature (T) anomalies (i.e., deviations from long-term averages by day-of-year) at 925 and 1,000 hPa were calculated. The results for the two pressure levels are similar, only results for 925 hPa are shown in the following. In all these composites the T anomaly patterns are consistent with advection of climatological temperature fields in winter by the anomalous atmospheric circulations, which is similar to the effect of advection on Arctic amplification (Clark et al., 2021). Wind-chill associated with the cold air outbreaks could be significant but is not estimated in this study.

Figure 7 shows the composite T anomalies (925 hPa) during long-duration WP+, WP-, PNA+ and PNA- events (N = 63, 68, 57, and 59, respectively, for 613, 674, 557, and 643 days). Large positive (negative) T anomalies over Canada are associated with the WP+ (WP-) events, with amplitudes up to nearly 10 K. The anomalies are generally a few Kelvins in amplitude in the most populated area from Chicago to Toronto and Quebec (Figures 7a and 7b). Opposite T anomalies over Alaska and the eastern half of the US are associated with the PNA events (Figures 7c and 7d). The largest T anomalies are found in the Great Lakes region: -5.7 K during PNA+ and 4.2 K during PNA- for an average duration of about 10 days. In the eastern half of North America, the number of cold

FAN ET AL. 9 of 21

21698996, 2024, 11, Downloaded from https://agupubs.onlinelibrary.wiley.com/doi/10.1029/2023JD039868 by Universitaet Leipzig, Wiley Online Library on [04/07/2024]. See the Terms

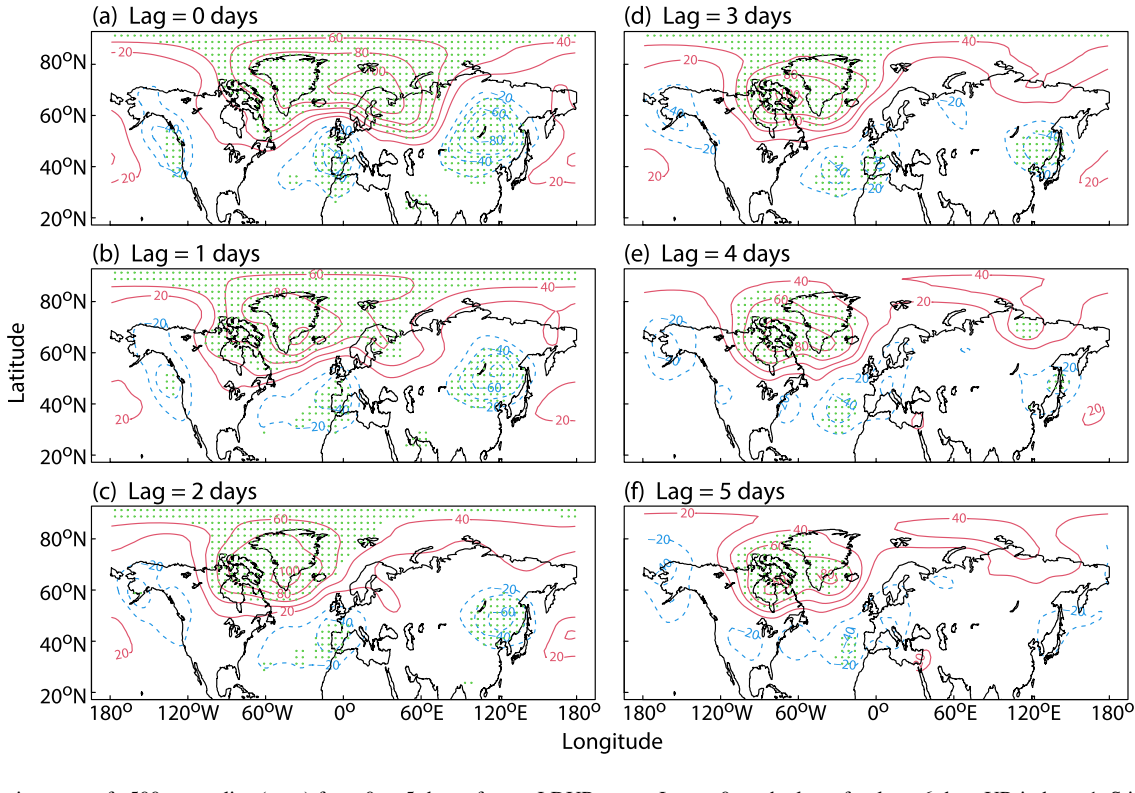


Figure 5. Composite mean of z500 anomalies (gpm) from 0 to 5 days after an LDUR event. Lag = 0 on the last of at least 6 days UR index >1. Stippling indicates significance at a global p-value of 1% level based on a field significance test.

events lasting >10 days increased from 1990 to 2004 to 2005–2019: from 5 to 11 for WP— and from 3 to 8 for PNA+ weather regimes, respectively (Table A2).

5.2. East Asia Cold Air Outbreaks Associated With LDUR

Figure 8 shows the composite T anomalies at 0–5 days after the end of LDUR events (N = 69, for a total of 703 days over 40 winters). The cold anomalies are largest near Lake Baikal at day 0 (Figure 8a, -6 K). Afterward the cold anomalies advance to Southeast China and to Korea and Japan, and persist to day 5 (Figures 8b–8f). The average length is about 15 days for cold anomalies associated with an LDUR. At the same time warm anomalies occur in the area near Baffin Bay (Figure 8), which result from a reduced cold advection associated with a ridge anomaly over the same area (Figure 5). The ridge anomaly is a remnant of westward extension of the UR (Figure 5).

In contrast to LDUR, negative T (925 hPa) anomalies after SD UR events can reach northeast, but not southeast, China (not shown). Previously Chen et al. (2018) showed composite-mean surface air temperature anomalies at time lags from -8 to 10 days from peak UB that is quasi-stationary, or followed by positive z500 anomalies moving westward and eastward. In terms of T anomalies in East Asia, our results for LDUR are comparable to eastward events, and SDUR to quasi-stationary events. Furthermore, cold anomalies are maximum near Lake Baikal in our UR composites, but over Central Eurasia (near the Caspian Sea) in their UB composites. This likely indicates that the UB events overlap more with the SCA than the UR/PEU patterns. More studies are needed to understand the differences between our UR and their UB composites.

Cold winters in Central Eurasia (40°N–60°N, 50°E–70°E or 60°E–120°E) were prevailing during 1966–1976 when SIC in the Nordic seas were higher than 1979–2019 (Luo et al., 2022; Yao et al., 2017). We extended our EOF analysis to 1948–1979 using the NCEP/NCAR reanalysis data and the Hadley Center seaice data. Significant differences are found for the frequencies of UR (23 vs. 39 for D1, 25 vs. 14 for D2) and UT (23 vs. 47 for D1, 2 vs. 9 for D3) following 15 low and 15 high SIC in the Nordic seas in autumn during 1948–1979. More UT events following a high autumn SIC contribute to a winter-mean warm bias over central to east Asia, which

FAN ET AL. 10 of 21

21698996, 2024. 11, Downloaded from https://aguputs.onintellbrary.wiley.com/doi/10.1029/2023JD039868 by Universtated Leipzig, Wiley Online Library on [0407/2024]. See the Terms and Conditions (https://onlinelibrary.wiley.com/terms-and-conditions) on Wiley Online Library for rules of use; OA articles are governed by the applicable Creat

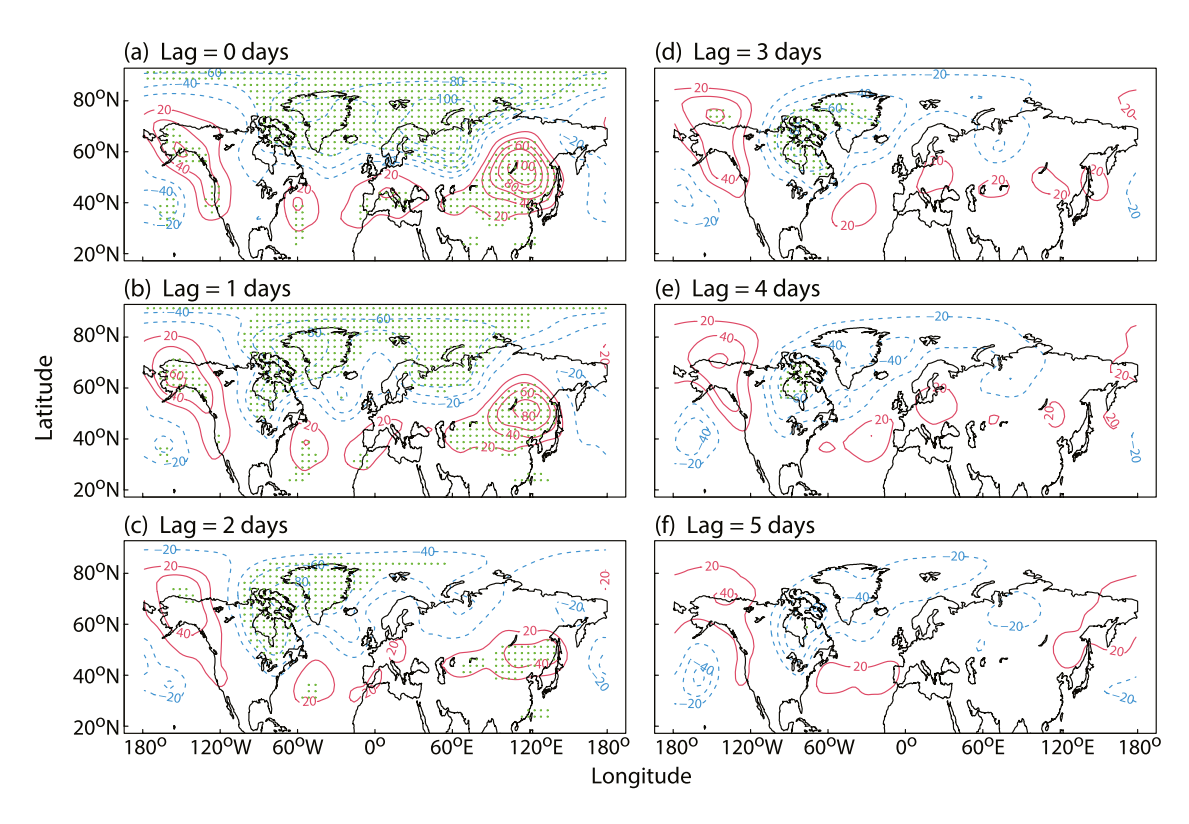


Figure 6. Composite mean of z500 anomalies (gpm) from 0 to 5 days after an LDUT event. Lag = 0 on the last of at least 6 days UT index > 1 (or URI < -1). Stippling indicates significance at a global p-value of 1% level based on a field significance test.

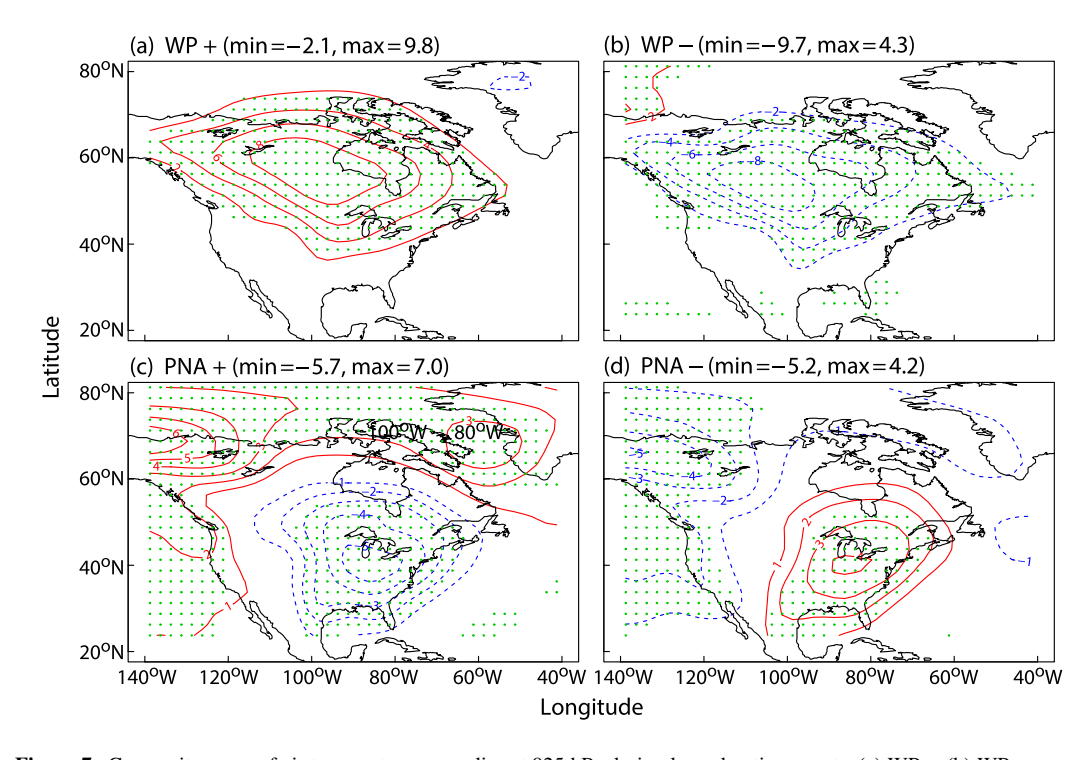


Figure 7. Composite mean of air temperature anomalies at 925 hPa during long-duration events. (a) WP+, (b) WP-, (c) PNA+, and (d) PNA-. Stippling indicates significance at a global *p*-value of 1% level based on a field significance test.

FAN ET AL. 11 of 21

21698996, 2024, 11, Downloaded from https://agupubs.onlinelibrary.wiley.com/doi/10.1029/2023JD039868 by Universitaet Leipzig, Wiley Online Library on [04/07/2024]. See the Terms

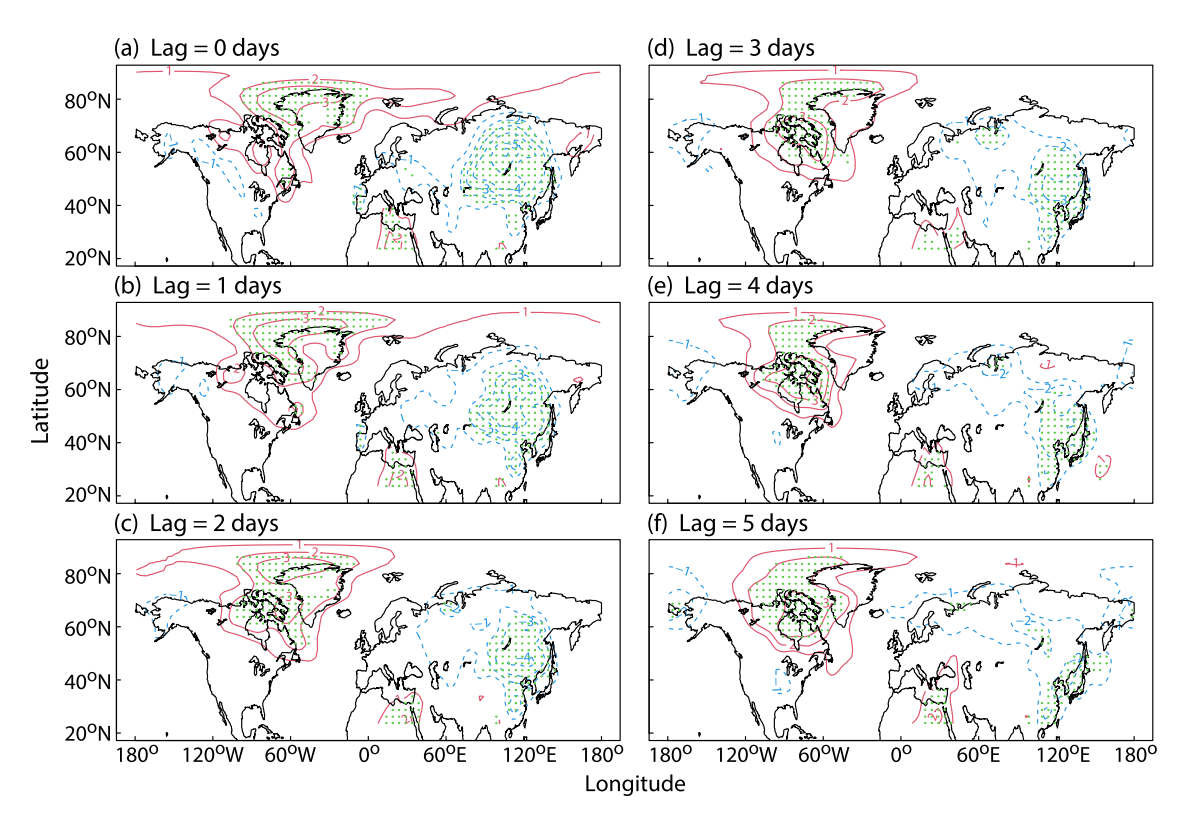


Figure 8. Composite mean of air temperature anomalies at 925 hPa 0-5 days after an LDUR event. Lag = 0 on the last of at least 6 days UR index > 1. Stippling indicates significance at a global p-value of 1% level based on a field significance test.

would have ameliorated the cold winters during 1966–1976. It was previously suggested that circulation changes due to the IPO— were responsible for the "background" cold winters during 1966–1976 (Luo et al., 2022). The 2000s was also a period of IPO— during which more UR events following a low autumn SIC would have worsened the cold winters from Central to East Asia. More UR events would also have enhanced the warm anomalies over the BKS associated with the AMO+ from 2004 to 2019 (Luo et al., 2022), contributing to the observed large Arctic amplification (Rantanen et al., 2022). However, 1–2 LDEs in a season have limited impact on the background winter-mean temperatures.

The decadal variations of the Indian Ocean basin mode are highly positively correlated with the IPO up to 1985, after which the correlation is weak (Dong & McPhaden, 2017). Negative SST anomalies between 1966 and 1976 were observed to be associated with the basin mode, while Indian Ocean-averaged (30°N–30°S, 40°–120°E) SST increased about 0.7°C over 70 years since 1950, with substantial contribution from external forcing (Dong & McPhaden, 2017). Modeling studies are needed to show whether these SST trends have contributed to colder temperatures from the Central Asia to Mongolia during 1966–1976 (Luo et al., 2022; Yao et al., 2017).

5.3. North America Cold Anomalies Associated With LDGR and LDUT

Figure 9 shows the composite T anomalies 1-4 days after the end of long-duration GR and GT events and 2-5 days after the end of long-duration UR and UT events (N=70, 54, 69, and 61, respectively). Opposite T anomalies over the eastern Canada and eastern US are found after the GR events (Figures 9a and 9b). The results shown in Figure 9a are consistent with previous studies. A blocking over the Baffin Bay and Greenland may force the polar jet to meander southward across the eastern half of the U.S., causing the arctic air mass to spill farther south (Ballinger et al., 2018; Overland & Wang, 2018). It may also cause a warm anomaly over the Davis Strait where SIC may be reduced as a result (Ballinger et al., 2018; Overland & Wang, 2018). In this study the cold anomalies in the eastern U.S. after an LDGR (Figure 9a) are attributed to the anomalous circulation resembling a PNA+ pattern (Figure 7c), while warm anomalies after an LDGT (Figure 9b) attributed to a weak ridge anomaly over the eastern U.S. (not shown).

FAN ET AL. 12 of 21

21698996, 2024, 11, Downloaded from https://agupubs.onlinelibrary.wiley.com/doi/10.1029/2023JD039868 by Universitaet Leipzig, Wiley Online Library on [04/07/2024]. See the Term

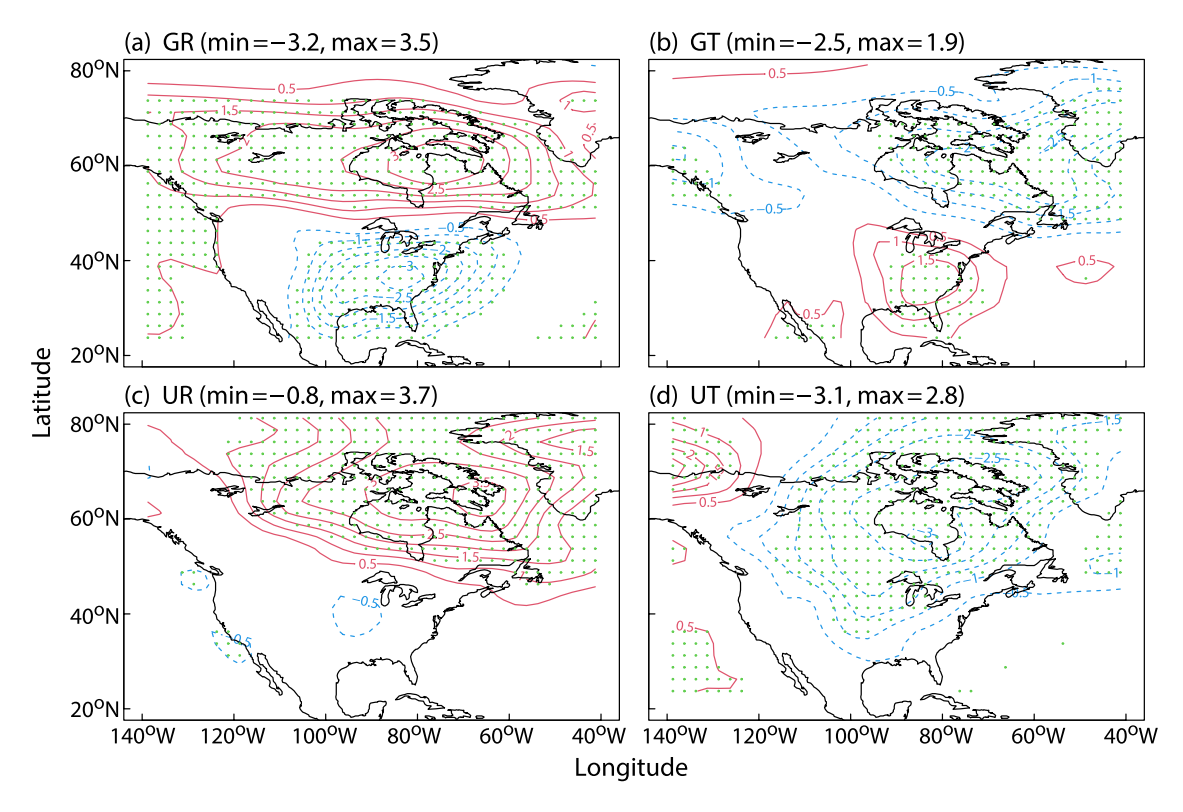


Figure 9. Composite mean of air temperature anomalies at 925 hPa 1–4 days after the end of long-duration GR (a) and GT (b) events, and 2–5 days after UR (c) and UT (d). Stippling indicates significance at a global *p*-value of 1% level based on a field significance test.

The first mode of Northern Hemisphere daily z500 from November to March (EOF1-NH) also shows a ridge centered over the southern tip of Greenland, a trough over the Pacific (center: $45^{\circ}N$ $150^{\circ}W$), and another trough over the North Atlantic ($35^{\circ}N$ $60^{\circ}W$) which extends to the eastern US (not shown); cold air moving down the west flank of the latter trough brings chill to the eastern US. The time series of daily PC1 in the AEA sector and PC1 for the NH are highly correlated (r = 0.84). Statistically a PNA+ pattern may persist for 2 weeks following an occurrence of EOF1-NH pattern based on their cross correlation (not shown).

Statistically significant positive T anomalies are found over eastern Canada after the LDUR events (Figure 9c), while negative T anomalies are found after the LDUT events in a greater area (extending from the Baffin Islands to the southern US (Figure 9d). The cold anomalies over North America after an LDUT are attributed to anomalous circulation associated with an Alaska-Hudson Bay dipole anomaly resembling a weak WP— pattern (Figure 6).

It is noteworthy that composite temperature anomalies are very small after short-duration UR/UT and GR/GT events. It is also noted that an overall increase of tropospheric temperature was reported over the eastern Canada from the 1990s to the 2000s, and attributed to circulation anomalies resembling an arched Rossby wave train in the upper troposphere originating from the tropical Pacific SST anomalies (Ding et al., 2014). Here we suggest that the T anomalies over the eastern Canada could also have resulted from increased UR and decreased UT events that may be associated with the reduction of SIC in the Nordic seas (Table 1).

5.4. Synoptical Variability Associated With the UR

In the following we propose another mechanism for the Arctic-North America tele-connection. It is well documented that synoptic Rossby waves can propagate from the North Atlantic over Eurasia and further eastward to the western Pacific where they seed new disturbances (e.g., Blackmon et al., 1984; Change & Yu, 1999; Joung & Hitchman, 1982). Synoptic waves can interfere with the quasi-stationary waves in the PNA sector (Goss et al., 2016), and can also cause atmospheric rivers reaching the west coast of North America (Prince et al., 2021). However, in the presence of Ural ridge/blocking, cyclones tend to move northward over the subarctic North

FAN ET AL. 13 of 21

21698996, 2024, 11, Downloaded from https://agupubs.onlinelibrary.wiley.com/doi/10.1029/2023JD039868 by Universitaet Leipzig, Wiley Online Library on [04/07/2024]. See the Terms

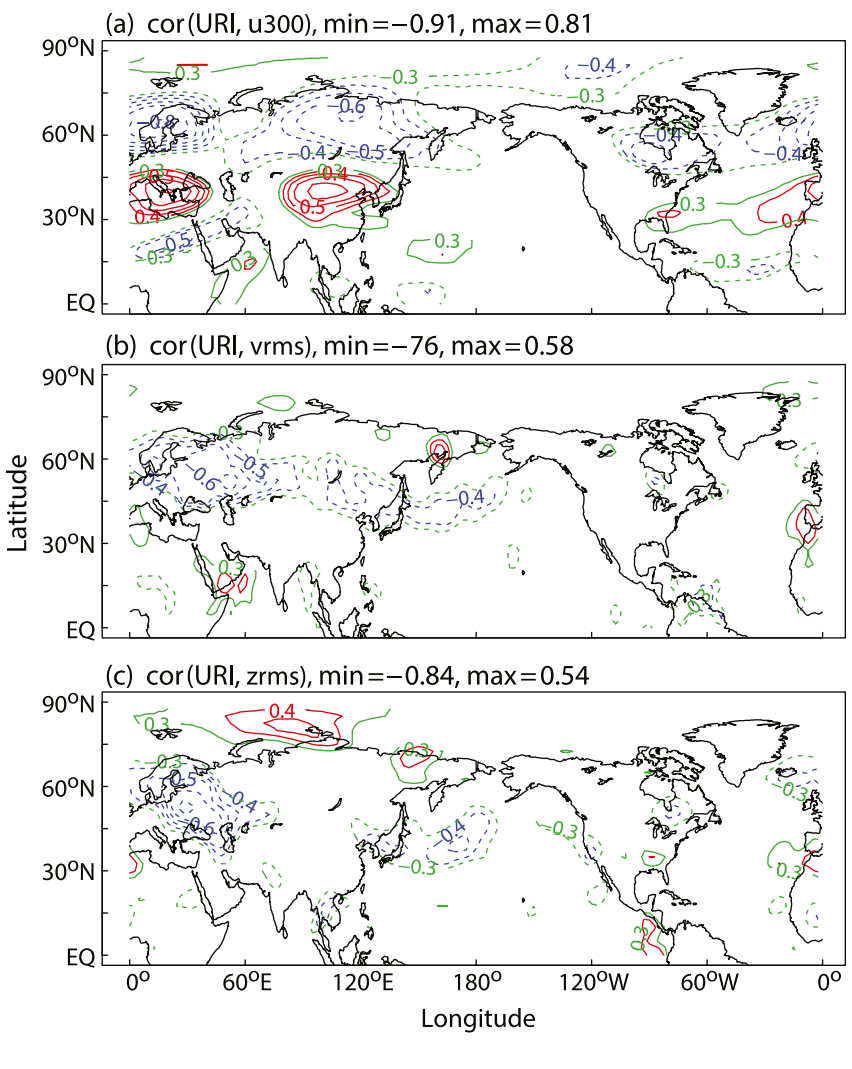


Figure 10. Correlation coefficient between the seasonal (DJF) mean Ural ridge index (URI) and zonal wind at 300 hPa (u300), between URI and root-mean-square (rms) of the band-passed meridional wind at 300 hPa (vrms), and between URI and rms of the band-passed geopotential height at 500 hPa (zrms). Red and blue contours, p = 0.01 at $r = \pm 0.4$; green contours: p = 0.06 at $r = \pm 0.3$.

Atlantic or Scandinavia and further into the Arctic rather than eastward over the mid-latitude Eurasia. It is shown in Figure 10 the correlation coefficients (r) between the URI and u300, the root-mean-square of bandpass (2.5–6 days) filtered meridional winds at 300 hPa (vrms) and z500 (zrms). All the daily time series data were averaged over the winter months (DJF), and the correlation coefficients were calculated for the time series of seasonal mean with the linear trends removed (N = 40, p = 0.01 at $r = \pm 0.4$, and p = 0.06 at $r = \pm 0.3$ indicated by green lines in Figure 10).

There are significant negative correlations between the URI and u300 over Scandinavia and Siberia (Figure 10a). The north-south dipoles of correlations (Figure 10a) are consistent with the east and west troughs associated with the UR pattern (Figure 1b). The positive correlations from Florida to the Mediterranean Sea are similar to increased zonal winds during NAO— or GR (Athanasiadis et al., 2010; Wettstein & Wallace, 2010).

Significant negative correlations between the URI and vrms are found from Eurasia to the western Pacific (near 45° N, up to the dateline, Figure 10b), indicating that an increase of UR events is correlated with a decrease of synoptic waves propagating from the mid-latitude Eurasia to the North Pacific. With Ural ridge a decrease of the synoptic disturbances over the North Pacific is also shown by the negative correlations between the URI and zrms, with a correlation of -0.4 shown along the coast of California (Figure 10c). It is interesting to study whether this mechanism has contributed to winter precipitation variations in California.

FAN ET AL. 14 of 21

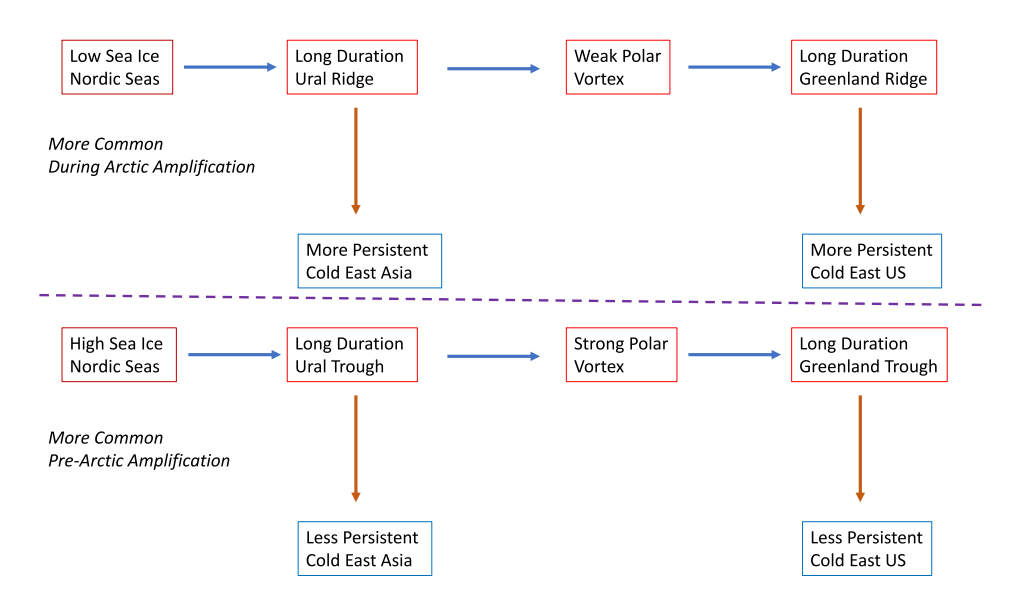


Figure 11. A schematic of the events made more likely by low or high sea ice cover in the Nordic seas. The blue arrows suggest sequential increases of probability and the red arrows indicate weather impacts.

6. Summary

In this study we define eight weather regimes in the extratropical Northern Hemisphere based on the EOF analysis of daily z500 anomalies from November to March during the 1979–2019 period. Because some extreme weather events are related to the long-duration (LD, >5 days) circulation patterns, the occurrences of these regimes were identified by periods with |PC| > 1, and grouped by duration (6–10, 11–15, >15 days). SD (1–5 days) events were also identified. Some significant changes were found about the frequency of occurrence and persistence for the weather regimes between years with high and low autumn sea ice in the Nordic seas, and from 1990 to 2004 to 2005–2019, including an increase of UR and weak PV (PVI < -1) and a decrease of UT and strong PV (PVI > 1) events. Strong evidence is thus provided for a causal connection between the decreasing SIC in the Nordic seas in autumn and increased occurrences of the UR and weak polar vortex in winter. This and other main results are summarized in Figure 11, and described as follows.

First, LD events of UR, weak PV and GR are all increased significantly following low autumn SIC. The LDUR events are associated with weak PV through advection of relatively warm air masses from North Atlantic into the Arctic as the ridge is strengthened. A weak PV promotes the development of LDGR. Frequent/persistent UR occurrences in winter suppress synoptic Rossby waves propagating from the North Atlantic to Japan and the western North Pacific. Conversely, simultaneous increases of UT, strong PV, and GT days may occur after high autumn SIC in the Nordic seas. A strong PV promotes LDUT and SDUT, as well as LDGT and SDGT. The LDUT events are associated with a cold Arctic and warm Eurasia pattern, and increased propagation of synoptic waves from the North Atlantic to the Pacific.

Secondly, it is shown that cold spells in East Asia persist for 5 more days after an LDUR event. The cold anomalies extend to Japan and southeast China after the LDUR events, while the extension of cold anomalies is limited to northeast China after the SDUR events. Cold anomalies from Canada to the U.S. occur 2–5 days after an LDUT event, and are associated with a z500 anomaly dipole centered over Alaska (+) and the Hudson Bay (–). Cold anomalies in the eastern U.S. may occur due to Greenland blocking (i.e., LDGR or EOF1-NH pattern), lasting more than 4 days after an LDGR due to circulations resembling the PNA+ pattern. In the eastern half of North America, the number of cold events lasting >10 days increased from 1990 to 2004 to 2005–2019: from 5 to 11 for WP— and from 3 to 8 for PNA+ weather regimes, respectively. However, the cause for this increase of extra-long cold events is uncertain.

It is necessary to note that the effect of Arctic SIC on the circulation patterns (weak/strong PV, UR/UT, GR/GT) emerging in our analysis should be considered as a modification of their "background" occurrence frequencies and durations. Because the circulation patterns are influenced by many local and remote processes on a range of

FAN ET AL. 15 of 21

time scales (synoptic to mutli-decadal), including the impact of global warming. Nevertheless, it is interesting that a surface forcing from decreasing SIC in the Nordic seas contributes substantially to the Arctic warming amplification, and can increase the number of episodic cold weather extremes in the mid latitudes, by largely modifying the natural modes of variability in atmospheric circulation.

In conclusion, natural and anthropogenic changes in SIC in the Nordic seas may impact the winter weather in Eurasia and North America through the extratropical circulation patterns. It has been suggested in literature that Arctic SIC and Eurasia snow cover in autumn may provide a source of weather predictability in winter (e.g., Furtado et al., 2016). Seasonal forecast of the Arctic SIC has seen marked improvement in recent years due to advances in sea-ice initialization and model development (Bushuk et al., 2022). This improvement could lead to more accurate forecasts of the long-duration weather regimes, cyclones and baroclinic wave activity on subseasonal-to-seasonal timescales (Zhang et al., 2021; Zheng et al., 2019).

Appendix A

Table A1Numbers of Events for Each Weather Regime by Durations in 15 High Ice Years (H) and 15 Low Ice Years (L), Respectively, During the Months November—March From 1979 to 2019

During the Months I	vovember–m	aren From 1;	9/9 10 2019							
	D1	D2	D3	D4	D1	D2	D3	D4		
Durations (days)	1–5	6–10	11–15	15+	1–5	6–10	11–15	15+		
		(GR		GT					
s.d.	5.8	3.1	1.9	1.4	9.0	4.1	2.3	0.6		
Н	52	19	6	2	55	11	4	1		
L	35	21	6	2	71	18	3	0		
	UR				UT					
s.d.	6.1	4.4	3.1	1.5	5.4	3.4	2.6	1.6		
Н	36	10	7	2	37	14	8	4		
L	35	26	10	4	33	11	4	2		
	WP+					WP-				
s.d.	7.2	3.7	2.5	1.3	6.9	3.7	2.4	1.3		
Н	44	21	4	3	34	19	7	1		
L	33	11	7	2	47	11	10	2		
	PNA+				PNA-					
s.d.	7.8	2.6	2.1	1.6	7.7	3.6	1.9	1.8		
Н	65	18	1	4	43	10	2	2		
L	41	10	7	2	53	19	6	5		
	Strong PV					Weak PV				
s.d.	4.9	2.6	1.7	1.7	4.7	1.9	1.6	2.2		
Н	19	2	3	4	9	3	4	5		
L	11	7	4	3	19	5	3	8		

Note. Sea ice concentrations were averaged from 30°W to 90°E and north of 70°N during the months December–February. Bold fonts signify a change greater than 2 standard deviations (s.d.). *High ice years:* DJF'89, 82, 98, 97, 88, 86, 81, 96, 04, 80, 87, 03, 99, 90, 92. *Low ice years:* DJF'17, 12, 16, 13, 18, 06, 19, 08, 07, 14, 10, 05, 85, 09, 84. *Medium ice years:* DJF'00, 02, 15, 83, 11, 95, 91, 01, 93, 94.

FAN ET AL. 16 of 21

21698996, 2024, 11, Downloaded from https://agupubs.onlinelibrary.wiley.com/doi/10.1029/2023JD039868 by Universitaet Leipzig, Wiley Online Library on [0407/2024]. See the Terms and Conditions (https://agupubs.onlinelibrary.wiley.com/doi/10.1029/2023JD039868 by Universitaet Leipzig, Wiley Online Library on [0407/2024]. See the Terms and Conditions (https://agupubs.onlinelibrary.wiley.com/doi/10.1029/2023JD039868 by Universitaet Leipzig, Wiley Online Library on [0407/2024]. See the Terms and Conditions (https://agupubs.onlinelibrary.wiley.com/doi/10.1029/2023JD039868 by Universitaet Leipzig, Wiley Online Library on [0407/2024]. See the Terms and Conditions (https://agupubs.onlinelibrary.wiley.com/doi/10.1029/2023JD039868 by Universitaet Leipzig, Wiley Online Library on [0407/2024]. See the Terms and Conditions (https://agupubs.onlinelibrary.wiley.com/doi/10.1029/2023JD039868 by Universitaet Leipzig, Wiley Online Library on [0407/2024]. See the Terms and Conditions (https://agupubs.onlinelibrary.wiley.com/doi/10.1029/2023JD039868 by Universitaet Leipzig, Wiley Online Library on [0407/2024]. See the Terms and Conditions (https://agupubs.onlinelibrary.wiley.com/doi/10.1029/2023JD039868 by Universitaet Leipzig, Wiley Online Library on [0407/2024]. See the Terms and Conditions (https://agupubs.onlinelibrary.wiley.com/doi/10.1029/2023JD039868 by Universitaet (https://agupubs.

Table A2Numbers of Events for Each Weather Regime by Durations in Two Periods, 1990–2004 and 2005–2019 (January Year), Respectively, During the Months November–March

Durations (days)	D1 1–5	D2 6–10	D3 11–15	D4 15+	D1 1–5	D2 6–10	D3 11–15	D4 15+		
		C	iR			(3T			
s.d.	5.8	3.1	1.9	1.4	9.0	4.1	2.3	0.6		
1990–2004	49	16	3	3	61	14	6	1		
2005–1019	37	20	5	3	77	17	3	0		
	UR				UT					
s.d.	6.1	4.4	3.1	1.5	5.4	3.4	2.6	1.6		
1990–2004	28	8	8	2	38	13	9	5		
2005–2019	41	23	8	3	36	13	2	2		
	WP+				WP-					
s.d.	7.2	3.7	2.5	1.3	6.9	3.7	2.4	1.3		
1990–2004	48	17	3	4	33	21	4	1		
2005–2019	34	8	6	2	49	15	8	3		
		PNA+				PNA-				
s.d.	7.8	2.6	2.1	1.6	7.7	3.6	1.9	1.8		
1990–2004	55	21	1	2	50	13	5	4		
2005–2019	40	11	7	1	60	18	6	4		
	Strong PV				Weak PV					
s.d.	4.9	2.6	1.7	1.7	4.7	1.9	1.6	2.2		
1990–2004	21	5	2	5	19	2	4	5		
2005–2019	10	10	4	2	19	6	4	7		

Note. Bold fonts signify a change greater than 2 standard deviations (s.d.).

Data Availability Statement

All data used in this study is publicly available. The geopotential height, air temperature, and wind data were obtained from the National Center for Environmental Prediction and Department of Energy (NCEP/DOE) reanalysis (https://psl.noaa.gov/data/gridded/data.doe.reanalysis.html) (Kanamitsu et al., 2002). The monthly sea-ice data were provided by the National Snow and Ice Data Center (https://nsidc.org/data/) at the University of Colorado Boulder (Meier et al., 2013; Peng et al., 2013). The NCEP and NCAR reanalysis data is available at (https://psl.noaa.gov/data/gridded/data.ncep.reanalysis.html) (Kalney et al., 1996). The sea ice data set from the Hadley Center is available at (https://www.metoffice.gov.uk/hadobs/hadisst/) (Rayner et al., 2003). Conventional daily teleconnection index data for NAO, PNA, and WP were obtained from the website (https://www.esrl.noaa.gov/psd/data/timeseries/daily/).

References

Athanasiadis, P., Wallace, J. M., & Wettstein, J. J. (2010). Patterns of wintertime jet stream variability and their relations to the storm track. Journal of the Atmospheric Sciences, 67(5), 1361–1381. https://doi.org/10.1175/2009JAS3270.1

Ballinger, T. J., Hanna, E., Hall, R. J., Miller, J., Ribergaard, M. H., & Hoyer, J. L. (2018). Greenland coastal air temperatures linked to Baffin Bay and Greenland Sea ice conditions during autumn through regional blocking patterns. *Climate Dynamics*, 50(1–2), 83–100. https://doi.org/10.1007/s00382-017-3583-3

Barnes, E. A. (2013). Revisiting the evidence linking Arctic amplification to extreme weather in midlatitudes. *Geophysical Research Letters*, 40(17), 4734–4739. https://doi.org/10.1002/grl.50880

Barnes, E. A., Samarasinghe, S. M., Ebert-Uphoff, I., & Furtado, J. C. (2019). Tropospheric and stratospheric causal pathways between the MJO and NAO. *Journal of Geophysical Research: Atmospheres*, 124(16), 9356–9371. https://doi.org/10.1029/2019jd031024

Barnes, E. A., & Screen, J. A. (2015). The impact of Arctic warming on the midlatitude jet-stream: Can it? Has it? Will it? WIREs Climate Change, 6(3), 277–286. https://doi.org/10.1002/wcc.337

Barnston, A. G., & Livezey, R. E. (1987). Classification, seasonality and persistence of low-frequency atmospheric circulation patterns. *Monthly Weather Review*, 115(6), 1083–1126. https://doi.org/10.1175/1520-0493(1987)115<1083:csapol>2.0.co;2

FAN ET AL. 17 of 21

Acknowledgments

2115072

suggestions that resulted in significant improvement of this manuscript. The author is grateful to Tom Knutson and John Lazante of GFDL for their many useful comments that led this manuscript from a draft of documentation to a completed investigation, including advices on statistical confidence estimation and an update of literature on the relationship (or a lack of) between arctic sea-ice and air temperature over the midlatitude land areas. Discussions with Xiaosong Yang of GFDL were also fruitful. Catherine Raphael helped with improving the graphics. JC is supported by the NSF Grants AGS-2140909 and ARCSS-

Dehai Luo and other reviewers provided

- Blackmon, M. L., Lee, Y.-H., Wallace, J. M., & Hsu, H.-H. (1984). Time variation of 500 mb height fluctuations with long, intermediate and short time scales as deduced from lag-correlation statistics. *Journal of the Atmospheric Sciences*, 41(6), 981–991. https://doi.org/10.1175/1520-0469 (1984)041<0981:tvomhf>2.0.co;2
- Blackport, R., & Screen, J. A. (2020). Insignificant effect of Arctic amplification on the amplitude of midlatitude atmospheric waves. *Science Advances*, 6(8), eaay2880. https://doi.org/10.1126/sciadv.aay2880
- Blackport, R., & Screen, J. A. (2021). Observed statistical connections overestimate the causal effects of Arctic sea ice changes on midlatitude winter climate. *Journal of Climate*, 34(8), 3021–3038. https://doi.org/10.1175/jcli-d-20-0293.1
- Blackport, R., Screen, J. A., van der Wiel, K., & Bintanja, R. (2019). Minimal influence of reduced Arctic sea-ice on coincident cold winters in mid-latitudes. *Nature Climate Change*, 9, 697–704. https://doi.org/10.1038/s41558-019-0551-4
- Bushuk, M., Zhang, Y., Winton, M., Hurlin, B., Delworth, T., Lu, F., et al. (2022). Mechanisms of regional Arctic Sea ice predictability in two dynamical seasonal forecast systems. *Journal of Climate*, 35(13), 4207–4231. https://doi.org/10.1175/JCLI-D-21-0544.1
- Butler, A. H., Sjoberg, J. P., Seidel, D. J., & Rosenlof, K. H. (2017). A sudden stratospheric warming compendium. *Earth System Science Data*, 9(1), 63–76. https://doi.org/10.5194/essd-9-63-2017
- Cassou, C. (2008). Intraseasonal interaction between the Madden-Julian oscillation and the North Atlantic oscillation. *Nature*, 455(7212), 523–527. https://doi.org/10.1038/nature07286
- Change, E. K. M., & Yu, D. B. (1999). Characteristics of wave packets in the upper troposphere. Part I: Northern Hemisphere winter. *Journal of the Atmospheric Sciences*, 56(11), 1708–1728. https://doi.org/10.1175/1520-0469(1999)056<1708:cowpit>2.0.co;2
- Chen, X., Luo, D., Feldstein, S. B., & Lee, S. (2018). Impact of winter Ural blocking on Arctic sea ice: Short-time variability. *Journal of Climate*, 31(6), 2267–2282. https://doi.org/10.1175/JCLI-D-17-0194.1
- Chen, X., Luo, D., Wu, Y., Dunn-Sigouin, E., & Lu, J. (2021). Nonlinear response of atmospheric blocking to early winter Barents-Kara Seas warming: An idealized model study. *Journal of Climate*, 34(6), 2367–2383. https://doi.org/10.1175/jcli-d-19-0720.1
- Chen, Y., Luo, D., Zhong, L., & Yao, Y. (2021). Effects of Barents–Kara Seas ice and North Atlantic tripole patterns on Siberian cold anomalies. Weather and Climate Extremes, 34, 100385. https://doi.org/10.1016/j.wace.2021.100385
- Cheung, H. N., Zhou, W., Shao, Y., Chen, W., Mok, H. Y., & Wu, M. C. (2012). Observational climatology and characteristics of wintertime
- atmospheric blocking over Ural-Siberia. Climate Dynamics, 41(1), 63–79. https://doi.org/10.1007/s00382-012-1587-6 Clark, J. P., Shenoy, V., Feldstein, S. B., Lee, S., & Goss, M. (2021). The role of horizontal temperature advection in Arctic amplification. Journal
- of Climate, 34(8), 2957–2976. https://doi.org/10.1175/jcli-d-19-0937.1 Cohen, J., Furtado, J. C., Jones, J., Barlow, M., Whittleston, D., & Entekhabi, D. (2014). Linking Siberian snow cover to precursors of strato-
- spheric variability. Journal of Climate, 27(14), 5422–5432. https://doi.org/10.1175/jcli-d-13-00779.1
- Cohen, J., Pfeiffer, K., & Francis, J. A. (2018). Warm Arctic episodes linked with increased frequency of extreme winter weather in the United States. *Nature Communications*, 9(1), 869. https://doi.org/10.1038/s41467-018-02992-9
- Cohen, J., Screen, J. A., Furtado, J. C., Barlow, M., Whittleston, D., Coumou, D., et al. (2014). Recent Arctic amplification and extreme mid-latitude weather. *Nature Geoscience*, 7(9), 627–637. https://doi.org/10.1038/ngeo2234
- Cohen, J., Zhang, X., Francis, J., Jung, T., Kwok, R., Overland, J., et al. (2020). Divergent consensuses on Arctic amplification influence on midlatitude severe winter weather. *Nature Climate Change*, 10(1), 20–29. https://doi.org/10.1038/s41558-019-0662-y
- Ding, Q., Wallace, J. W., Battisti, D. S., Steig, E. J., Gallant, A. J. E., Kim, H.-J., & Geng, L. (2014). Tropical forcing of the recent rapid Arctic warming in northeastern Canada and Greenland. *Nature*, 509(7499), 209–213. https://doi.org/10.1038/nature13260
- Dong, L., & McPhaden, M. J. (2017). Why has the relationship between Indian and Pacific Ocean decadal variability changed in recent decades? Journal of Climate, 30(6), 1971–1983. https://doi.org/10.1175/JCLI-D-16-0313.1
- Fan, S. (2022). The Influence of extratropical weather regimes on wintertime temperature variations in the Arctic during 1979–2019. *Atmosphere*, 13(6), 880. https://doi.org/10.3390/atmos13060880
- Fan, S., & Yang, X. (2017). Arctic and East Asia winter climate variations associated with the eastern Atlantic pattern. *Journal of Climate*, 30(2), 573–583, https://doi.org/10.1175/jcli-d-15-0741.1
- Fletcher, C., Hardiman, S. C., Kushner, P. J., & Cohen, J. (2009). The dynamical response to snow cover perturbations in a large ensemble of atmospheric GCM integrations. *Journal of Climate*, 22(5), 1208–1222. https://doi.org/10.1175/2008JCLI2505.1
- Francis, J. A. (2017). Why are Arctic linkages to extreme weather still up in the air? Bulletin of the American Meteorological Society, 98(12),
- 2551–2557. https://doi.org/10.1175/BAMS-D-17-0006.1
 Francis, J. A., Skific, N., & Vavrus, S. J. (2018). North American weather regimes are becoming more persistent: Is Arctic amplification a factor? Geophysical Research Letters, 45(20), 11414–11422. https://doi.org/10.1029/2018GL080252
- Francis, J. A., Skific, N., & Vavrus, S. J. (2020). Increased persistence of large-scale circulation regimes over Asia in the era of amplified Arctic warming, past and future. *Scientific Reports*, 10(1), 14953. https://doi.org/10.1038/s41598-020-71945-4
- Francis, J. A., & Vavrus, S. J. (2012). Evidence linking Arctic amplification to extreme weather in mid-latitudes. *Geophysical Research Letters*, 39(6), L06801. https://doi.org/10.1029/2012GL051000
- Furtado, J. C., Cohen, J. L., & Tziperman, E. (2016). The combined influences of autumnal snow and sea ice on Northern Hemisphere winters. Geophysical Research Letters, 43(7), 3478–3485. https://doi.org/10.1002/2016GL068108
- García-Serrano, J., Frankignoul, C., Gastineau, G., & de la Cámara, A. (2015). On the predictability of the winter Euro-Atlantic climate: Lagged influence of autumn Arctic Sea ice. *Journal of Climate*, 28(13), 5195–5216. https://doi.org/10.1175/jcli-d-14-00472.1
- Gong, T., & Luo, D. (2017). Ural blocking as an amplifier of the Arctic sea ice decline in winter. Journal of Climate, 30(7), 2639–2654. https://doi.org/10.1175/jcli-d-16-0548.1
- Goss, M., Feldstein, S. B., & Lee, S. (2016). Stationary wave interference and its relation to tropical convection and Arctic warming. *Journal of Climete*, 20(4), 1360, 1389. https://doi.org/10.1175/feli.ed.15.0067.1
- Climate, 29(4), 1369–1389. https://doi.org/10.1175/jcli-d-15-0267.1 Groisman, P. Y. (1992). Possible regional climate consequences of the Pinatubo eruption: An empirical approach. Geophysical Research Letters,
- 19(15), 1603–1606. https://doi.org/10.1029/92gl01474
 Jenney, A. M., Nardi, K. M., Barnes, E. A., & Randall, D. A. (2019). The seasonality and regionality of MJO impacts on North American temperature. Geophysical Research Letters, 46(15), 1–10. https://doi.org/10.1029/2019GL083950
- Jiang, Y., Cheung, H.-N., Li, Y., & Yang, S. (2023). Intra-seasonal variation of the wintertime Polar/Eurasia pattern. Climate Dynamics, 61(1–2), 813–830. https://doi.org/10.1007/s00382-022-06612-7
- Joung, C. H., & Hitchman, M. H. (1982). On the role of successive downstream development in East Asian polar air outbreaks. Monthly Weather Review, 110(9), 1224–1237. https://doi.org/10.1175/1520-0493
- Kalney, E., Kanamitsu, M., Kistler, R., Collins, W., Deaven, D., Gandin, L., et al. (1996). The NCEP/NCAR 40-year reanalysis project [Dataset]. Bulletin of the American Meteorological Society, 77(3), 437–471. https://doi.org/10.1175/1520-0477

FAN ET AL. 18 of 21

- Kanamitsu, M., Ebisuzaki, W., Woollen, J., Yang, S.-K., Hnilo, J. J., Fiorino, M., & Potter, G. L. (2002). NCEP-DOE AMIP-II reanalysis (R-2) [Dataset]. Bulletin of the American Meteorological Society, 83(11), 1631–1643. https://doi.org/10.1175/bams-83-11-1631(2002)083<1631: nar>2.3.co;2
- Kim, B. M., Son, S. W., Min, S. K., Jeong, J. H., Kim, S. J., Zhang, X., et al. (2014). Weakening of the stratospheric polar vortex by Arctic sea-ice loss. *Nature Communications*, 5(1), 4646. https://doi.org/10.1038/ncomms5646
- Kim, J., & Kim, K.-Y. (2020). Characteristics of stratospheric polar vortex fluctuations associated with sea ice variability in the Arctic winter. Climate Dynamics, 54(7–8), 3599–3611. https://doi.org/10.1007/s00382-020-05191-9
- Kumar, V., Yoden, S., & Hitchman, M. H. (2022). QBO and ENSO effects on the mean meridional circulation, polar vortex, subtropical westerly jets, and wave patterns during boreal winter. *Journal of Geophysical Research: Atmospheres*, 127(15), e2022JD036691. https://doi.org/10.1029/2022JD036691
- Labe, Z., Peings, Y., & Magnusdottir, G. (2019). The effect of QBO phase on the atmospheric response to projected Arctic sea ice loss in early winter. Geophysical Research Letters, 46(13), 7663–7671. https://doi.org/10.1029/2019GL083095
- Leathers, D. J., Yarnal, B., & Palecki, M. A. (1991). The Pacific/North America teleconnection pattern and United States climate. Part I: Regional temperature and precipitation associations. *Journal of Climate*, 4(5), 517–528. https://doi.org/10.1175/1520-0442(1991)004<0517:tpatpa>2.0. co:2
- Lee, S., Gong, T., Feldstein, S. B., Screen, J. A., & Simmonds, I. (2017). Revisiting the cause of the 1989–2009 Arctic surface warming using the surface energy budget: Downward infrared radiation dominates the surface fluxes. *Geophysical Research Letters*, 44(20), 10654–10661. https://doi.org/10.1002/2017GL075375
- Lee, S., Gong, T., Johnson, N., Feldstein, S. B., & Pollard, D. (2011). On the possible link between tropical convection and the Northern Hemisphere Arctic surface air temperature change between 1958 and 2001. *Journal of Climate*, 25(16), 4350–4367. https://doi.org/10.1175/2011jcli4003.1
- Lin, H., Brunet, G., & Yu, B. (2015). Interannual variability of the Madden-Julian oscillation and its impact on the North Atlantic oscillation in the boreal winter. Geophysical Research Letters, 42(13), 5571–5576. https://doi.org/10.1002/2015GL064547
- Livezey, R. E., & Chen, W. Y. (1983). Statistical field significance and its determination by Monte Carlo techniques. *Monthly Weather Review*, 111(1), 46–59. https://doi.org/10.1175/1520-0493
- Luo, D., Dai, A., Simmonds, I., & Wu, L. (2022). The modulation of interdecadal Pacific oscillation and Atlantic multidecadal oscillation on winter Eurasian cold anomaly via the Ural blocking change. Climate Dynamics, 59(1–2), 127–150. https://doi.org/10.1007/s00382-021-06119-7
- Luo, B., Luo, D., Wu, L., Zhong, L., & Simmonds, I. (2017). Atmospheric circulation patterns which promote winter Arctic sea ice decline. Environmental Research Letters, 12(5), 054017. https://doi.org/10.1088/1748-9326/aa69d0
- Luo, D., Chen, X., Dai, A., & Simmonds, I. (2018). Changes in atmospheric blocking circulations linked with winter Artic warming: A new perspective. *Journal of Climate*, 31, 7661–7677.
- Luo, D., Chen, X., Overland, J., Simmonds, I., Wu, Y., & Zhang, P. (2019). Weakened potential vorticity barrier linked to recent winter Arctic sea ice loss and midlatitude cold extremes. *Journal of Climate*, 32(14), 4235–4261. https://doi.org/10.1175/jcli-d-18-0449.1
- Luo, D., Xiao, Y., Yao, Y., Dai, A., Simmonds, I., & Franzke, C. (2016). Impact of Ural blocking on winter warm Arctic-cold Eurasian anomalies. Part I: Blocking induced amplification. *Journal of Climate*, 29(11), 3925–3947. https://doi.org/10.1175/jcli-d-15-0611.1
- Matsumura, S., & Kosaka, Y. (2019). Arctic-Eurasian climate linkage induced by tropical ocean variability. *Nature Communications*, 10(1), 3441. https://doi.org/10.1038/s41467-019-11359-7
- McCusker, K. E., Fyfe, J. C., & Sigmond, M. (2016). Twenty-five winters of unexpected Eurasian cooling unlikely due to Arctic sea-ice loss. Nature Geoscience, 9(11), 838–842. https://doi.org/10.1038/ngeo2820
- McKenna, C. M., Bracegirdle, T. J., Shuckburgh, E. F., Haynes, P. H., & Joshi, M. M. (2018). Arctic sea ice loss in different regions leads to contrasting Northern Hemisphere impacts. *Geophysical Research Letters*, 45(2), 945–954. https://doi.org/10.1002/2017GL076433
- Meier, W., Fetterer, F., Savoie, M., Mallory, S., Duerr, R., & Stroeve, J. (2013). NAOA/NSIDC climate data record of passive microwave sea ice concentration, Version 2; National snow and ice data center: Boulder, CO, USA [Dataset]. https://nsidc.org/data/
- Mori, M., & Watanabe, M. (2008). The growth and triggering mechanisms of the PNA: An MJO-PNA coherence. *Journal of the Meteorological Society of Japan*, 86(1), 213–236. https://doi.org/10.2151/jmsj.86.213
- Mori, M., Watanabe, M., Shiogama, H., Inoue, J., & Kimoto, M. (2014). Robust Arctic sea-ice influence on the frequent Eurasian cold winters in past decades. *Nature Geoscience*, 7(12), 869–873. https://doi.org/10.1038/ngeo2277
- Murto, S., Caballero, R., Svensson, G., & Papritz, L. (2022). Interaction between Atlantic cyclones and Eurasian atmospheric blocking drives wintertime warm extremes in the high Arctic. Weather Climate Dynamics, 3(1), 21–44. https://doi.org/10.5194/wcd-3-21-2022
- Nakamura, T., Yamazaki, K., Iwamoto, K., Honda, M., Miyoshi, Y., Ogawa, Y., et al. (2016). The stratospheric pathway for Arctic impacts on midlatitude climate. Geophysical Research Letters, 43(7), 3494–3501. https://doi.org/10.1002/2016GL068330
- Nakamura, T., Yamazaki, K., Iwamoto, K., Honda, M., Miyoshi, Y., Ogawa, Y., & Ukita, J. (2015). A negative phase shift of the winter AO/NAO due to the recent Arctic sea-ice reduction in late autumn. *Journal of Geophysical Research: Atmospheres*, 120(8), 3209–3227. https://doi.org/10.1002/2014jd022848
- Nishi, K., Nakamura, H., & Orsolini, Y. J. (2010). Cooling of the winter Arctic stratosphere induced by western Pacific teleconnection pattern. Geophysical Research Letters, 37, L13805. https://doi.org/10.1029/2010GL043551
- Overland, J. E. (2016). A difficult Arctic science issue: Midlatitude weather linkages. *Polar Science*, 10(3), 210–216. https://doi.org/10.1016/j.polar.2016.04.011
- Overland, J. E., Ballinger, T. J., Cohen, J., Francis, J. A., Hanna, E., Jaiser, R., et al. (2021). How do intermittency and simultaneous processes obfuscate the Arctic influence on midlatitude winter extreme weather events? *Environmental Research Letters*, 16(4), 043002. https://doi.org/10.1088/1748-9326/abdb5d
- Overland, J. E., Dethloff, K., Francis, J. A., Hall, R. J., Hanna, E., Kim, S.-J., et al. (2016). Nonlinear response of mid-latitude weather to the changing Arctic. *Nature Climate Change*, 6(11), 992–998. https://doi.org/10.1038/nclimate3121
- Overland, J. E., & Wang, M. (2018). Arctic-midlatitude weather linkages in North America. *Polar Science*, 16, 1–9. https://doi.org/10.1016/j.polar.2018.02.001
- Pang, B., Scaife, A. A., Lu, R., Ren, R., & Zhao, X. (2023). Interdecadal variations of the Scandinavian pattern. *Journal of Climate*, 36(10), 3275–3288. https://doi.org/10.1175/JCLI-D-22-0494.1
- Peings, Y. (2019). Ural blockings as a driver of early-winter stratospheric warmings. Geophysical Research Letters, 46(10), 5460–5468. https://doi.org/10.1029/2019gl082097
- Peings, Y., Davini, P., & Magnusdottir, G. (2023). Impact of Ural blocking on early winter climate variability under different Barents-Kara sea ice conditions. *Journal of Geophysical Research: Atmospheres*, 128(6), e2022JD036994. https://doi.org/10.1029/2022JD036994

FAN ET AL. 19 of 21

- Peings, Y., Labe, Z. M., & Magnusdottir, G. (2021). Are 100 ensemble members enough to capture the remote atmospheric response to +2°C Arctic sea ice loss? *Journal of Climate*, 34(10), 3751–3769. https://doi.org/10.1175/JCLI-D-20-0613.1
- Peng, G., Meier, W., Scott, D., & Savoie, M. (2013). A long-term and reproducible passive microwave sea ice concentration data record for climate studies and modeling [Dataset]. Earth System Science Data, 5(2), 311–318. https://doi.org/10.5194/essd-5-311-2013
- Peng, S., Robinson, W. A., & Li, S. (2002). North Atlantic SST forcing of the NAO and relationships with intrinsic hemispheric variability. Geophysical Research Letters, 29(8), 1276. https://doi.org/10.1029/2001GL014043
- Peng, S., Robinson, W. A., & Li, S. (2003). Mechanisms for the NAO responses to the North Atlantic SST tripole. *Journal of Climate*, 16(12), 1987–2004. https://doi.org/10.1175/1520-0442(2003)016<1987:mftnrt>2.0.co;2
- Perlwitz, J., & Graf, H.-F. (2001). Troposphere-stratosphere dynamic coupling under strong and weak polar vortex conditions. *Geophysical Research Letters*, 28(2), 271–274. https://doi.org/10.1029/2000gl012405
- Prince, H. D., Gibson, P. B., DeFlorio, M. J., Corringham, T. W., Cobb, A., & Guan, B., et al. (2021). Genesis locations of the costliest atmospheric rivers impacting the western United States. *Geophysical Research Letters*, 48(20), e2021GL093947. https://doi.org/10.1029/2021GL093947
- Rantanen, M., Karpechko, A. Y., Lipponen, A., Nordling, K., Hyvärinen, O., Ruosteenoja, K., et al. (2022). The Arctic has warmed nearly four times faster than the globe since 1979. Communications Earth and Environment, 3(1), 168. https://doi.org/10.1038/s43247-022-00498-3
- Rayner, N. A., Parker, D. E., Horton, E. B., Folland, C. K., Alexander, L. V., Rowell, D. P., et al. (2003). Global analysis of sea surface temperature, sea ice, and night marine air temperature since the late nineteenth century [Dataset]. *Journal of Geophysical Research*, 108(D14), 4407. https://doi.org/10.1029/2002JD002670
- Riddle, E. E., Stoner, M. B., Johnson, N. C., L'Heureux, M. L., Collins, D. C., & Feldstein, S. B. (2013). The impact of the MJO on clusters of wintertime circulation anomalies over the North American region. *Climate Dynamics*, 40(7–8), 1749–1766. https://doi.org/10.1007/s00382-012-1493-y
- Robertson, A. W., & Ghil, M. (1999). Large-scale weather regimes and local climate over the Western United States. *Journal of Climate*, 12(6), 1796–1813. https://doi.org/10.1175/1520-0442(1999)012<1796:lswral>2.0.co;2
- Robock, A. (2000). Volcanic eruptions and climate. Review of Geophysics, 38(2), 191-219. https://doi.org/10.1029/1998rg000054
- Roundy, P. E., MacRitchie, K., Asuma, J., & Melino, T. (2010). Modulation of the global atmospheric circulation by combined activity in the Madden-Julian Oscillation and the El Niño-Southern Oscillation during boreal winter. *Journal of Climate*, 23(15), 4045–4059. https://doi.org/10.1175/2010jcli3446.1
- Stenchikov, G., Robock, A., Ramaswamy, V., Schwarzkopf, M. D., Hamilton, K., & Ramachandran, S. (2002). Arctic Oscillation response to the 1991 Mount Pinatubo eruption: Effects of volcanic aerosols and ozone depletion. *Journal of Geophysical Research*, 107(D24), 4803. https://doi.org/10.1029/2002JD002090
- Sun, L., Deser, C., Simpson, I., & Sigmond, M. (2022). Uncertainty in the winter tropospheric response to Arctic sea ice loss: The role of stratospheric polar vortex internal variability. *Journal of Climate*, 35(10), 3109–3130. https://doi.org/10.1175/JCLI-D-21-0543.1
- Sun, L., Deser, C., & Tomas, R. A. (2015). Mechanisms of stratospheric and tropospheric circulation response to projected Arctic sea ice loss. Journal of Climate, 28(19), 7824–7845. https://doi.org/10.1175/JCLI-D-15-0169.1
- Sung, M.-K., Jang, H.-Y., Kim, B.-M., Yeh, S.-W., Choi, Y.-S., & Yoo, C. (2019). Tropical influence on the North Pacific oscillation drives winter extremes in North America. *Nature Climate Change*, 9(5), 413–418. https://doi.org/10.1038/s41558-019-0461-5
- Thompson, D. W. J., & Wallace, J. M. (2001). Regional climate impacts of the Northern Hemisphere annular mode. *Science*, 293(5527), 85–89. https://doi.org/10.1126/science.1058958
- Tibaldi, S., & Molteni, F. (1990). On the operational predictability of blocking. *Tellus*, 42(3), 343–365. https://doi.org/10.1034/j.1600-0870.1990. t01-2-00003.x
- Tyrlis, E., Manzini, E., Bader, J., Ukita, J., Nakamura, H., & Matei, D. (2019). Ural blocking driving extreme Arctic sea ice loss, cold Eurasia, and stratospheric vortex weakening in autumn and early winter 2016-2017. *Journal of Geophysical Research: Atmospheres*, 124(21), 11313—11329. https://doi.org/10.1029/2019JD031085
- Vavrus, S. J., Wang, F., Martin, J., Francis, J., Peings, Y., & Cattiaux, J. (2017). Changes in North American atmospheric circulation and extreme weather: Influence of Arctic amplification and northern hemisphere snow cover. *Journal of Climate*, 30(11), 4317–4333. https://doi.org/10.1175/JCLI-D-16-0762.1
- Wallace, J. M., & Gutzler, D. S. (1981). Teleconnections in the potential height field during the Northern Hemisphere winter. *Monthly Weather Review*, 109(4), 784–812. https://doi.org/10.1175/1520-0493(1981)109<0784:titghf>2.0.co;2
- Wang, M., & Tan, B. (2020). Two types of the Scandinavian pattern: Their formation mechanisms and climate impacts. *Journal of Climate*, 33(7), 2645–2661. https://doi.org/10.1175/JCLI-D-19-0447.1
- Warner, J. L., Screen, J. A., & Scaife, A. A. (2020). Links between Barents-Kara sea ice and the extratropical atmospheric circulation explained by internal variability and tropical forcing. *Geophysical Research Letters*, 47(1), e2019GL085679. https://doi.org/10.1029/2019GL085679
- Wettstein, J. J., & Wallace, J. M. (2010). Observed patterns of month-to-month storm track variability and their relationship to the background flow. *Journal of the Atmospheric Sciences*, 67(5), 1420–1437. https://doi.org/10.1175/2009JAS3194.1
- Wilks, D. S. (2016). "THE stippling shows statistically significant grid points" how Research results are routinely overstated and overinterpreted, and what to do about it. *Bulletin of the American Meteorological Society*, 97(12), 2263–2273. https://doi.org/10.1175/bams-d-15-00267.1
- Wise, E. K., Wrzesien, M. L., Dannenberg, M. P., & McGinnis, D. L. (2015). Cool-season precipitation patterns associated with teleconnection interactions in the United States. *Journal of Applied Meteorology and Climatology*, 54(2), 494–505. https://doi.org/10.1175/jamc-d-14-0040.1
- Woo, S.-H., Sung, M.-K., Son, S.-W., & Kug, J.-S. (2015). Connection between weak stratospheric vortex events and the Pacific Decadal Oscillation. Climate Dynamics, 45(11–12), 3481–3492. https://doi.org/10.1007/s00382-015-2551-z
- Xiang, B., Harris, L., Delworth, T., Wang, B., Chen, G., Chen, J. H., et al. (2021). S2S prediction in GFDL SPEAR: MJO diversity and tele-connections. Bulletin of the American Meteorological Society, 103(2), 1–46. https://doi.org/10.1175/BAMS-D-21-0124.1
- Yang, X., Delworth, T., Jia, L., Lu, F., Johnson, N., & McHugh, C. (2022). On the seasonal prediction and predictability of winter surface temperature swing index Over North America. Frontiers in Climate, 4. https://doi.org/10.3389/fclim.2022.972119
- Yao, Y., Luo, D., Dai, A., & Simmonds, I. (2017). Increased quasi-stationarity and persistence of Ural blocking and Eurasian extreme cold events in response to Arctic warming. Part I: Insight from Observational Analyses. *Journal of Climate*, 30(10), 3549–3568. https://doi.org/10.1175/ jcli-d-16-0261
- You, C., Tjernström, M., Devasthale, A., & Steinfeld, D. (2022). The role of atmospheric blocking in regulating Arctic warming. Geophysical Research Letters, 49(12), e2022GL097899. https://doi.org/10.1029/2022g1097899
- Zhang, G., Murakami, H., Cooke, W., Wang, Z., Jia, L., Lu, F., et al. (2021). Seasonal predictability of baroclinic wave activity. npj Climate and Atmospheric Science, 4(1), 50. https://doi.org/10.1038/s41612-021-00209-3

FAN ET AL. 20 of 21

- Zhang, P., Wu, Y., Simpson, I. R., Smith, K. L., Zhang, X., De, B., & Callaghan, P. (2018). A stratospheric pathway linking a colder Siberia to Barents-Kara Sea ice loss. *Science Advances*, 4(7), eaat6025. https://doi.org/10.1126/sciadv.aat6025
- Zhang, X., Lu, C., & Guan, Z. (2012). Weakened cyclones, intensified anticyclones and recent extreme cold winter weather events in Eurasia. Environmental Research Letters, 7(4), 044044. https://doi.org/10.1088/17489326/7/4/044044
- Zheng, C., Chang, E., Kim, H., Zhang, M., & Wang, W. (2019). Subseasonal to seasonal prediction of wintertime northern hemisphere extratropical cyclone activity by S2S and NMME models. *Journal of Geophysical Research: Atmospheres*, 124(22), 12057–12077. https://doi.org/10.1029/2019JD031252
- Zhou, S., L'Heureux, M., Weaver, S., & Kumar, A. (2012). A composite study of the MJO influence on the surface air temperature and precipitation over the Continental United States. *Climate Dynamics*, 38(7–8), 1459–1471. https://doi.org/10.1007/s00382-011-1001-9

FAN ET AL. 21 of 21